ORIGINAL ARTICLE

Gut commensal *Parabacteroides goldsteinii* plays a predominant role in the anti-obesity effects of polysaccharides isolated from *Hirsutella sinensis*

Tsung-Ru Wu,[1,2] Chuan-Sheng Lin,[1,3,4,5,6] Chih-Jung Chang,[1,3,4,5,6] Tzu-Lung Lin,[1] Jan Martel,[3,5] Yun-Fei Ko,[5,7,8] David M Ojcius,[3,5,9] Chia-Chen Lu,[10] John D Young,[3,5,7,8,11] Hsin-Chih Lai[1,3,4,5,6,12,13,14]

► Additional material is published online only. To view, please visit the journal online (http://dx.doi.org/10.1136/gutjnl-2017-315458).

For numbered affiliations see end of article.

Correspondence to
Dr John D Young, Center for Molecular and Clinical Immunology, Chang Gung University, Gueishan, Taoyuan 33302, Taiwan; jdyoung@mail.cgu.edu.tw and Dr Hsin-Chih Lai, Department of Medical Biotechnology and Laboratory Science, College of Medicine, Chang Gung University, Gueishan, Taoyuan 33302, Taiwan ; hclai@mail.cgu.edu.tw

T-RW, C-SL and C-JC contributed equally.

Received 13 October 2017
Revised 22 June 2018
Accepted 22 June 2018
Published Online First
14 July 2018

© Author(s) (or their employer(s)) 2019. No commercial re-use. See rights and permissions. Published by BMJ.

To cite: Wu T-R, Lin C-S, Chang C-J, *et al*. *Gut* 2019;**68**:248–262.

ABSTRACT

Objective The medicinal fungus *Ophiocordyceps sinensis* and its anamorph *Hirsutella sinensis* have a long history of use in traditional Chinese medicine for their immunomodulatory properties. Alterations of the gut microbiota have been described in obesity and type 2 diabetes. We examined the possibility that *H. sinensis* mycelium (HSM) and isolated fractions containing polysaccharides may prevent diet-induced obesity and type 2 diabetes by modulating the composition of the gut microbiota.

Design High-fat diet (HFD)-fed mice were treated with HSM or fractions containing polysaccharides of different molecular weights. The effects of HSM and polysaccharides on the gut microbiota were assessed by horizontal faecal microbiota transplantation (FMT), antibiotic treatment and 16S rDNA-based microbiota analysis.

Results Fraction H1 containing high-molecular weight polysaccharides (>300 kDa) considerably reduced body weight gain (~50% reduction) and metabolic disorders in HFD-fed mice. These effects were associated with increased expression of thermogenesis protein markers in adipose tissues, enhanced gut integrity, reduced intestinal and systemic inflammation and improved insulin sensitivity and lipid metabolism. Gut microbiota analysis revealed that H1 polysaccharides selectively promoted the growth of *Parabacteroides goldsteinii*, a commensal bacterium whose level was reduced in HFD-fed mice. FMT combined with antibiotic treatment showed that neomycin-sensitive gut bacteria negatively correlated with obesity traits and were required for H1's anti-obesogenic effects. Notably, oral treatment of HFD-fed mice with live *P. goldsteinii* reduced obesity and was associated with increased adipose tissue thermogenesis, enhanced intestinal integrity and reduced levels of inflammation and insulin resistance.

Conclusions HSM polysaccharides and the gut bacterium *P. goldsteinii* represent novel prebiotics and probiotics that may be used to treat obesity and type 2 diabetes.

Significance of this study

What is already known on this subject?

- Diet-induced dysbiosis and leaky gut contribute to the development of obesity and type 2 diabetes.
- Polysaccharides derived from medicinal fungi such as *Ganoderma lucidum* reduce weight gain in obese mice.
- *Hirsutella sinensis* mycelium (HSM) produces anti-inflammatory, hypoglycaemic and lipid-lowering effects in animals.

What are the new findings?

- High-molecular weight polysaccharides (>300 kDa) derived from HSM produce anti-obesogenic and antidiabetic effects in obese mice.
- HSM polysaccharides reverse obesity-induced gut dysbiosis and leaky gut, and reduce metabolic endotoxemia, inflammation, insulin resistance and dyslipidemia.
- HSM polysaccharides modulate the composition of the gut microbiota, notably by enriching the gut bacterium *Parabacteroides goldsteinii*.
- Oral treatment of obese mice with live *P. goldsteinii* bacteria prevents body weight gain, improves intestinal integrity and reduces inflammation and insulin resistance.

How might it impact on clinical practice in the foreseeable future?

- High-molecular weight polysaccharides derived from HSM represent novel prebiotics to treat obesity and type 2 diabetes.
- *P. goldsteinii* is a novel probiotic bacterium that may be used to treat obesity and associated metabolic disorders.

INTRODUCTION

Obesity is a metabolic disorder associated with increased risk of developing type 2 diabetes mellitus, cardiovascular disease and cancer.[1–4] Obesity is characterised by body weight gain, accumulation of fat tissues, gut microbiota dysbiosis,[5] leaky gut,[6] metabolic endotoxemia,[6 7] chronic inflammation,[6 8] insulin resistance[6 9 10] and adipocyte hypertrophy.[11] Excess body weight also contributes to the development of non-alcoholic fatty liver disease (NAFLD) and non-alcoholic steatohepatitis (NASH).[9]

Recent studies indicate that gut microbiota dysbiosis is associated with disrupted gut barrier function and metabolic endotoxemia.[12–15] Strategies that restore the gut microbiota have thus been proposed to prevent and treat obesity.[16–19] Diet represents a critical factor that affects host metabolism by modulating the gut microbiota.[20] Several studies have shown that modulation of the gut microbiota using prebiotics and probiotics may improve intestinal integrity and host metabolism and reduce obesity and chronic inflammation.[17 21–24] Polysaccharides and dietary fibre can reduce body weight and exert anti-inflammatory effects by enhancing the growth of specific anti-obesogenic gut bacteria and the production of microbiota-derived metabolites.[25–27] However, further studies are needed to better understand the complex interactions between diet, prebiotics and the gut microbiota.

Many herbal remedies used in traditional Chinese medicine (TCM) exert anti-obesogenic and antidiabetic effects.[28] One class of traditional remedies consists of medicinal fungi, such as *Ophiocordyceps sinensis* and *Ganoderma lucidum*, which contain a wide range of immunomodulatory and bioactive compounds.[29–32] We previously observed that *G. lucidum* reduces obesity in high-fat diet (HFD)-fed mice by modulating the composition of the gut microbiota.[33] The caterpillar fungus, *O. sinensis* (also called cordyceps), and its anamorph, *Hirsutella sinensis*, also produce immunomodulatory, anti-inflammatory, hypoglycaemic and lipid-lowering effects,[34 35] but the possibility that this fungus may induce anti-obesogenic effects has not been examined.

In the present study, we show that a water extract of *H. sinensis* mycelium (HSM) and polysaccharide-containing fractions isolated from the extract reduce body weight and accumulation of fat tissues in a murine model of diet-induced obesity. Further experiments showed that neomycin-sensitive bacteria including *Parabacteroides goldsteinii* are required for the anti-obesogenic effects of HSM polysaccharides. Thus, our results reveal the existence of a new commensal bacterial species responsible for the anti-obesogenic effects of fungal polysaccharides.

METHODS

Animal experiments

Four-week-old C57BL/6J male mice were purchased from the NARLab facility (Taiwan). Animals were housed four to five individuals per cage with free access to food and sterile drinking water (DW) (reverse osmosis grade) in a temperature-controlled room (21°C±2°C) under a 12 hours dark-light cycle. After an accommodation period of 1 week, mice were fed for 12 weeks with standard chow diet (chow, 13.5% of energy from fat; LabDiet 5001; LabDiet, USA) or HFD (60% of energy from fat; TestDiet 58Y1; TestDiet, USA). Mice were supplemented daily with 100 µL of sterile saline (vehicle), HSM (20 mg/kg) or polysaccharide fractions H1–H4 (20 mg/kg) by intragastric gavage. At the time indicated, non-fasting animals were anaesthetised and whole blood was withdrawn by cardiac puncture. Visceral adipose tissues (ie, epididymal white adipose tissues) and the liver were removed and weighed. Organs and tissues were immersed in liquid nitrogen and stored at −80°C for further analysis.

Preparation of HSM water extract and polysaccharides

H. sinensis strain CGB 999335 was isolated and cultured as described previously.[36] HSM consisted of <10% crude fibre; >3% polysaccharides; crude proteins at 42.8 g/100 g; crude fat at 8.2 g/100 g; carbohydrates at 31.9 g/100 g; amino acids at 7.8 g/100 g and sodium at 242.7 mg/100 g. Calories were measured at 373 kcal per 100 g. HSM water extract and polysaccharide fractions were prepared as described earlier for *G. lucidum*.[33]

Measurement of serum cytokines

Whole blood was withdrawn by cardiac puncture in tubes containing no anticoagulant (BD, USA). Blood was allowed to clot for 30 min. Solutions were centrifuged at 15 000 *g* for 1 min and supernatants (serum) were collected. ELISA kits were used to measure interleukin (IL)-1β and tumour necrosis factor-alpha (TNF-α) from serum according to the manufacturer's instructions (R&D Systems, USA).

Serum endotoxin detection

Serum endotoxin was quantified using a *Limulus amaebocyte* lysate (LAL) kit (Cambrex Bio Science, USA) according to the manufacturer's instructions.

Briefly, serum samples were diluted 1:10 to 1:1000 in endotoxin-free water (Lonza, USA), heated at 70°C for 10–15 min and processed according to the manufacturer's protocol. Recovery rate was determined based on the net lipopolysaccharide (LPS) concentration of spiked samples supplemented with LPS (0.1 EU/mL, Sigma, USA). Samples with a recovery rate of at least 50% were considered.

Measurement of homeostatic model assessment-insulin resistance index

Fasting blood glucose was measured using glucometer strips (Johnson & Johnson Medical Devices, Hong Kong) as done before.[37] Fasting insulin was measured using a commercial ELISA kit (Mercodia, Sweden). Homeostatic model assessment-insulin resistance (HOMA-IR) was calculated using the following equation: fasting glucose (mg/dL)×fasting insulin (µU/mL)/405.

In vivo intestinal permeability assay

Intestinal permeability was assessed in vivo following oral administration of fluorescein-isothiocyanate (FITC)-dextran (4 kDa; Sigma), a high molecular weight glucose polymer which, based on the information provided by the manufacturer, is neither digested nor absorbed by healthy mice. Animals were orally gavaged with FITC-dextran (44 mg/100 g), 4 hours before sacrifice. Whole blood was obtained by cardiac puncture before killing. Serum was diluted with phosphate-buffered saline (PBS) and fluorescence was monitored using a spectrophotofluorometer (Synergy HT, BioTek, USA) using excitation at 485 nm and emission at 528 nm. A standard curve was prepared based on a series of twofold dilution of FITC-dextran in PBS. Serum from mice that had not received FITC-dextran was used as background control.

In vitro Caco-2 cell monolayer permeability assay

Human Caco-2 cells were purchased from European Collection of Authenticated Cell Cultures (UK). Caco-2 cells were cultured in Dulbecco's modified Eagle's medium supplemented with 10% fetal bovine serum, 50 U/mL penicillin and streptomycin at 37°C under 5% CO_2. Caco-2 cells (1×10^5) were grown on polyethylene terephthalate membrane-based transwell plates (0.4 µm pores; Millipore, USA) for 21 days to reach confluence (transepithelial electrical resistance (TEER) >1000 Ωcm^2). Caco-2 monolayer grown on the apical side of transwells were treated with LPS (100 µg/mL; O111:B4, Sigma) and 1 mg/mL of H1 or 50 multiplicity of infection of *P. goldsteinii*. LPS diluted in serum-free medium served as a positive control, and serum-free

medium as vehicle control. TEER values were monitored for 12 hours using a Millicell-ERS-2 volt-ohm metre (Millipore).

Antibiotic treatment

For in vivo antibiotic treatment, HFD-fed mice were treated with either H1 or saline, combined with 50 µg/mL clindamycin (C) (Goldbio, USA), 50 µg/mL metronidazole (M) (Sigma), 50 µg/mL penicillin (P) (Sigma), 25 µg/mL vancomycin (V) (Sigma) and/or 50 µg/mL neomycin (N) (Sigma) in sterile DW for 12 weeks. For ex vivo faecal microbiota transplantation (FMT), HFD-fed mice (aged 5 weeks, male) were treated daily with H1 or saline by oral gavage for 6 weeks. During week 4 to week 6 (total of 14 days), faecal microbiota from each donor mouse was collected daily, treated with antibiotics, pooled, mixed and stored at –80°C. To prepare faecal microbiota, faeces pellets (150–180 mg) were collected daily in sterile tubes, prior to suspension and homogenisation in 1 mL of PBS. After centrifugation at 2000*g* at 4°C for 1 min, bacteria-enriched supernatants were collected and centrifuged 5 min at 15 000 g. Bacterial pellets were resuspended in 1 mL of sterile saline containing the antibiotics CMPV, neomycin or CMPVN, followed by stationary incubation under aerobic conditions at 37°C for 2 hours. After antibiotic treatment, faecal microbiota specimens were collected, washed twice with saline, resuspended in 700 µL of saline with 20% (v/v) glycerol and stored at –80°C. HFD-fed mice (aged 5 weeks, male) were treated daily with faecal microbiota transplants from each donor group via oral gavage for 12 weeks.

Caecal microbiota analysis

Caecal microbiota DNA was extracted using the QIAamp DNA Stool Mini Kit (Qiagen, USA) and applied to amplification of V3-V4 regions of 16S rDNA. Caecal microbiota composition was assessed using Illumina HiSeq sequencing of 16S rDNA amplicon and QIIME-based microbiota analysis. The detailed procedure of caecal microbiota DNA extraction, sequencing and library construction and microbiota analysis pipeline is described in the supplementary methods.

P. goldsteinii cultivation, preparation and treatment

P. goldsteinii (ATCC BAA-1180, also called JCM 13446) was purchased from the American Type Culture Collection (ATCC, USA). Bacteria were grown at 37°C in a Whitley DG250 anaerobic chamber (Don Whitley, UK) with mixed anaerobic gas (5% carbon dioxide, 5% hydrogen, 90% nitrogen). Anaerobicity was confirmed using an anaerobic indicator (Oxoid, UK). *P. goldsteinii* was cultivated on anaerobic blood agar (Creative, Taiwan) and liquid thioglycollate medium (BD). *P. goldsteinii* was collected by centrifugation and resuspended in sterile saline. Mice were treated daily with 4×10^7 colony-forming units of *P. goldsteinii* by oral gavage. Heat-killed or pasteurised *P. goldsteinii* were prepared by heating bacteria at 100°C for 15 min or 70°C for 30 min, respectively. Mice were treated daily with either heat-killed or pasteurised *P. goldsteinii* by oral gavage.

Statistical analysis

Statistical analysis was performed using GraphPad Prism V.7.0a (GraphPad Software, USA). Data are shown as means±SD and medians±IQR for parametric and non-parametric analysis, respectively. Differences between two groups were assessed using unpaired two-tailed Student's t-test. Data sets involving more than two groups were assessed by one-way analysis of variance (ANOVA) followed by Bonferroni's post hoc test or by the non-parametric Kruskal-Wallis test with Dunn's multiple comparisons test. Bacterial species with statistically significant difference were assessed using Metastats.[38] Levels of bacterial species showing statistically significant differences in Metastats data were also evaluated using the non-parametric Kruskal-Wallis test with false discovery rate (FDR) correction for multiple testing (<5%).[39] Correlation coefficients between bacterial species and obesity traits were determined using Spearman's correlation analysis. P values <0.05 were considered to be statistically significant. Where indicated in the figure legends, the method described by Benjamini *et al*[39] was also used to evaluate FDR (<5%) for estimated p values.

RESULTS

HSM and polysaccharide fractions reduce body weight in HFD-fed mice

To test the effects of HSM on body weight, we fed mice with an HFD for 12 weeks and supplemented the animals' diet with daily administration of HSM water extract or saline as negative control (see online supplementary figure S1A). Compared with the chow diet, mice fed an HFD showed increased body weight, visceral fat mass, liver weight, serum triglycerides and HOMA-IR index values (see online supplementary figure S1B-H). Notably, HSM significantly reduced these obesity traits in a dose-dependent manner (see online supplementary figure S1B-H).

To identify the compounds responsible for HSM's anti-obesogenic effects, we fractionated the HSM water extract into four fractions based on molecular weight (figure 1A and supplementary table S1). Administration of fraction H1, which contained polysaccharides with a molecular weight above 300 kDa (see online supplementary table S1), reduced body weight by ~50% after 12 weeks compared with HFD (figure 1B–D). Fraction H1 also reduced visceral fat and HOMA-IR index in HFD-fed mice, producing effects similar to those observed for the HSM water extract (figure 1E,F). While fraction H4 containing oligosaccharides and carbohydrates of low molecular weight did not affect body weight or obesity traits, fractions H2 (10–300 kDa) and H3 (<10 kDa) reduced visceral fat pad mass, but produced no effect on body weight or HOMA-IR index (figure 1B–F).

HSM-derived polysaccharides reduce metabolic disorders in HFD-fed mice

HSM and H1 did not affect energy intake (see online supplementary figure S2A) or fat absorption (see online supplementary figure S2B), indicating that these treatments did not modulate appetite or lipid absorption. In addition, HSM and H1 did not affect caecal or colonic production of short-chain fatty acids (SCFAs), such as acetate, propionate or butyrate (see online supplementary figure S3). On the other hand, HSM and H1 reduced serum triglycerides (see online supplementary figure S4A) and gene expression involved in lipolysis, lipid transport and uptake and lipogenesis in adipose and hepatic tissues (see online supplementary figure S4B,C). HSM and H1 enhanced gene expression associated with hepatic β-oxidation, compared with the HFD group (see online supplementary figure S4C, Acsl3). In comparison, fractions H2–H4 affected some but not all lipid metabolism parameters (see online supplementary figure S4).

HSM and H1–H3 treatment reduced fasting glucose compared with HFD, while only HSM and H1 reduced fasting insulin (see online supplementary figure S5A,B). HSM and fractions H1–H3 improved glucose tolerance in the oral glucose tolerance test (see online supplementary figure S5C,D), but

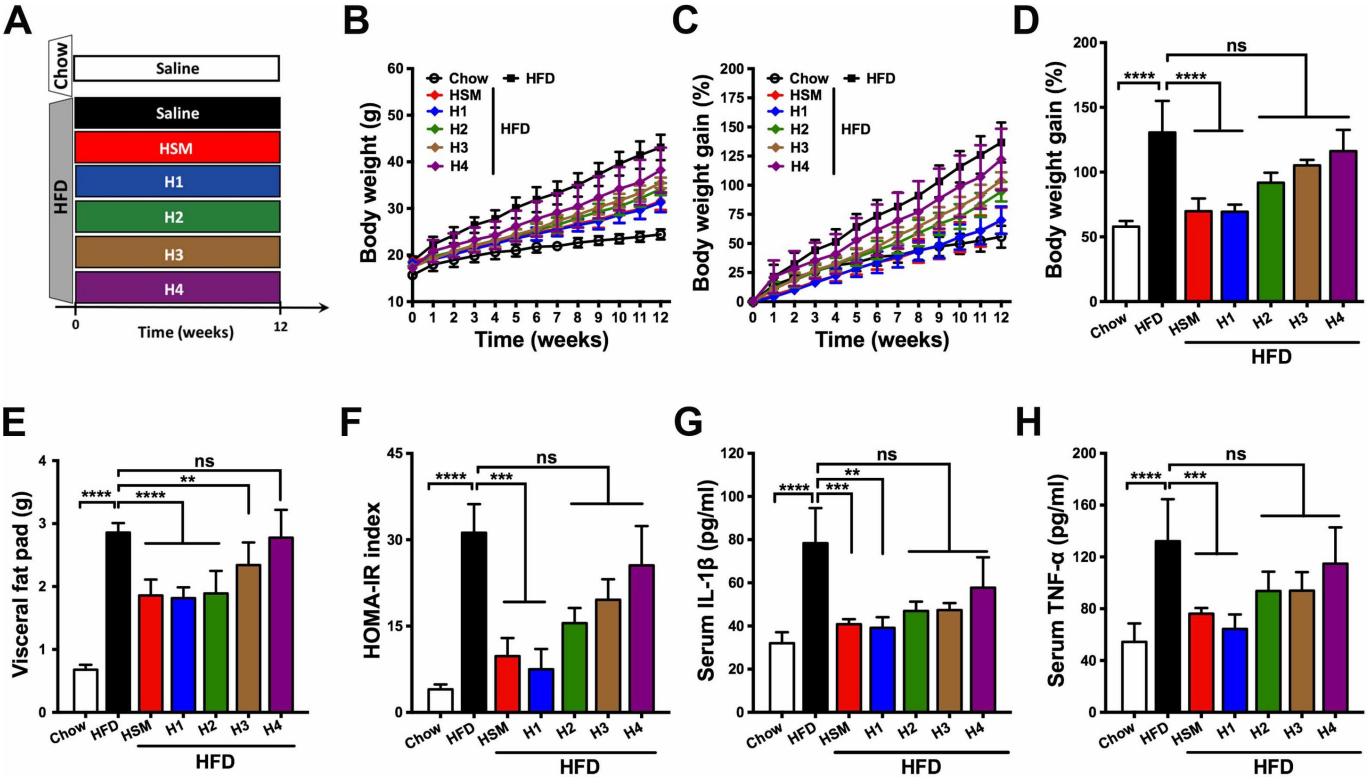

Figure 1 *Hirsutella sinensis* mycelium (HSM) and H1 reduce diet-induced obesity and metabolic disorders. (A) Chow-fed mice and high-fat diet (HFD)-fed mice were treated daily with control saline, HSM water extract (HSM) (20 mg/kg) or HSM-derived fractions (H1–H4) (20 mg/kg) for 12 weeks by oral gavage. (B) Body weight and (C) relative body weight were measured throughout the 12-week period. Obesity traits including (D) body weight gain, (E) visceral fat pad weight (epididymal white adipose tissue), (F) homeostatic model assessment-insulin resistance (HOMA-IR) index, (G) serum interleukin (IL)-1β and (H) serum tumour necrosis factor-alpha (TNF-α) were measured after 12 weeks of treatment as described in the 'Methods' section. Data are presented as means±SD from three independent experiments (n=10–15 mice per group). Statistical analysis was performed using one-way analysis of variance followed by Bonferroni's post hoc test and false discovery rate (FDR) correction for multiple testing. **p<0.01; ***p<0.001; ****p<0.0001; ns, not statistically significant.

only HSM and H1 improved insulin sensitivity in the insulin tolerance test (see online supplementary figure S5E, F).

HSM and H1 reduced serum levels of the pro-inflammatory cytokines IL-1β and TNF-α, compared with HFD (figure 1G,H). Consistent with the effects described above on lipid metabolism (see online supplementary figure S4), HSM and H1 reduced adipocyte hypertrophy and the number of crown-like structures (CLS)—tissue lesions in which macrophages surround dead adipocytes (see online supplementary figure S6). We monitored expression of mitochondrial uncoupling protein 1 (UCP1), which was identified earlier as a major regulator of thermogenesis in adipose tissues.[40] HSM and H1 increased UCP1 mRNA and protein expression in brown adipose tissues (BATs) and inguinal white adipose tissues (iWATs) compared with the HFD group (see online supplementary figure S7), suggesting that HSM and H1 may increase thermogenesis. Furthermore, HSM and H1 reduced signs of NAFLD and NASH, including liver cell hypertrophy and accumulation of lipid droplets, in the liver of HFD-fed mice (see online supplementary figure S8 and supplementary dataset S1). While HSM and H1 produced a modest but statistically significant reduction of body weight in chow-fed mice, the treatments did not affect visceral fat weight, HOMA-IR index or pro-inflammatory cytokine levels in this group (see online supplementary figure S9). These results indicate that HSM and H1 produce anti-obesogenic, antidiabetic and anti-inflammatory effects in HFD-fed mice.

HSM and H1 prevent leaky gut and metabolic endotoxemia

Previous studies have shown that an HFD reduces expression of intestinal tight junction proteins (eg, zonula occludens-1 (ZO-1)) and disrupts gut barrier integrity, leading to translocation of bacterial LPS into the blood (ie, metabolic endotoxemia) and producing inflammation and insulin resistance.[5–7 15 41] Notably, HSM and H1 significantly reduced serum endotoxin levels (figure 2A) and intestinal permeability (figure 2B) in HFD-fed mice. These observations were accompanied by increased expression of ZO-1 (figure 2C) and reduced mRNA expression of pro-inflammatory cytokines (figure 2D,E) in the colon of mice treated with HSM or H1. In contrast, fractions H2–H4 failed to reverse serum endotoxemia (figure 2A), intestinal permeability (figure 2B) or expression of colonic pro-inflammatory cytokines or ZO-1 (figure 2C–E). HSM and H1 significantly increased levels of regulatory T cells expressing the anti-inflammatory cytokine IL-10 in colonic lamina propria of HFD-fed mice (figure 2F), while reducing levels of M1 macrophages expressing pro-inflammatory IL-1β (figure 2G). In addition, H1 reduced LPS-induced disruption of cell monolayers (figure 2H, measured using the TEER assay)

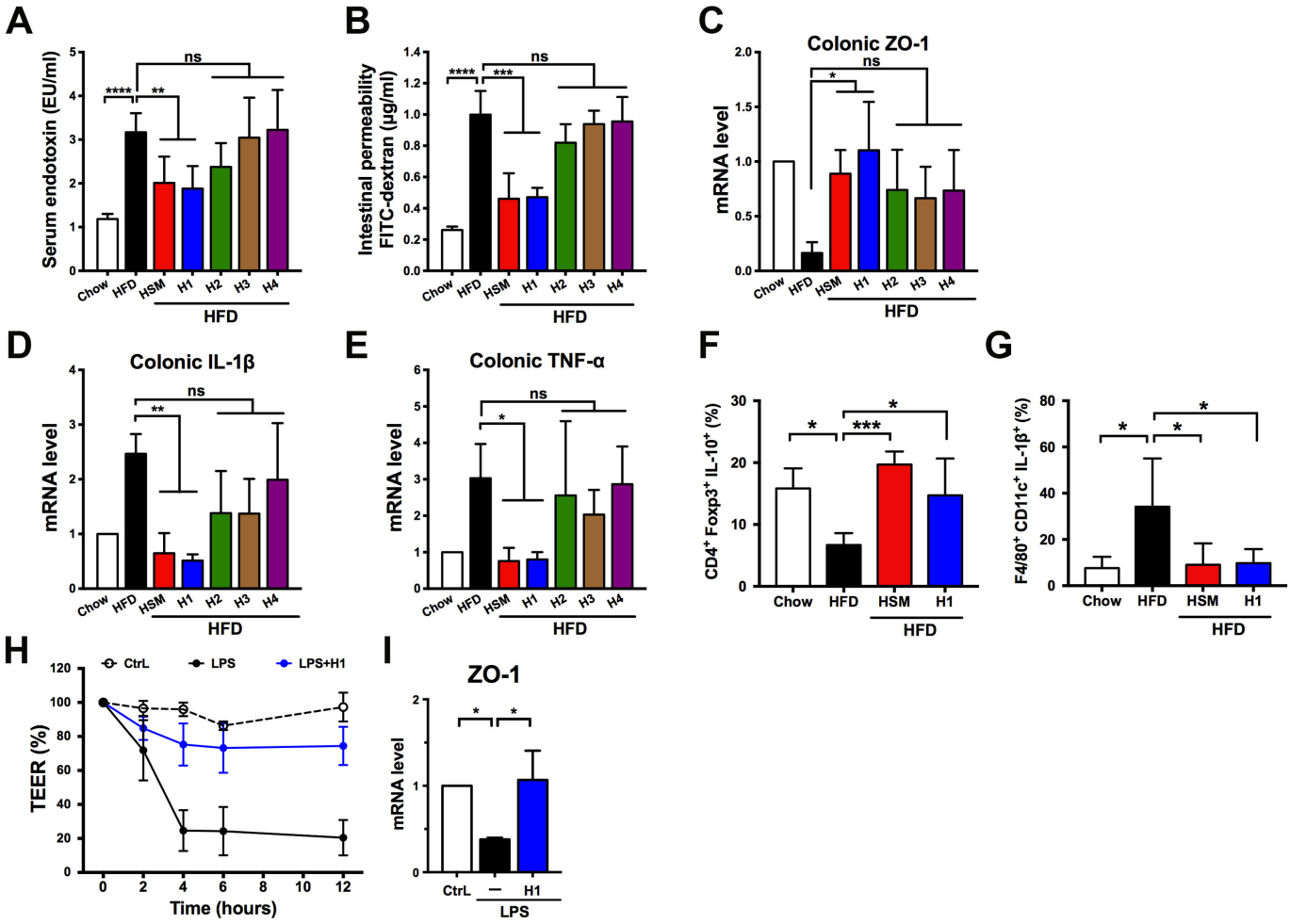

Figure 2 *Hirsutella sinensis* mycelium (HSM) and H1 improve intestinal integrity and produce immunomodulatory effects. Experiments were performed as in figure 1. (A) Serum endotoxin and (B) intestinal permeability were measured as described in the 'Methods' section. (C) Zonula occludens-1 (ZO-1), (D) interleukin (IL)-1β and (E) tumour necrosis factor-alpha (TNF-α) expression in proximal colon was examined using quantitative real-time PCR (qRT-PCR). Expression levels were normalised to glyceraldehyde 3-phosphate dehydrogenase and expressed as relative fold changes compared with the chow group. Levels of (F) IL-10-expressing regulatory T cells and (G) IL-1β-expressing M1 macrophages were analysed using flow cytometry. (H) In vitro Caco-2 cell permeability was monitored using the transepithelial electrical resistance (TEER) assay. (I) ZO-1 expression in Caco-2 cells was examined using qRT-PCR. Caco-2 cells were treated with control (CtrL) serum-free medium, lipopolysaccharide (LPS) or LPS plus H1 for 12 hours. Expression levels were normalised to 18S rRNA and expressed as relative fold changes compared with the vehicle control. Data are presented as means±SD from three independent experiments (A, B, n=10–15 mice/group; H, I, duplicate/group) or two independent experiments (C–G; n=5–10 mice per group). Statistical analysis was performed using one-way analysis of variance followed by Bonferroni's post hoc test and false discovery rate correction for multiple testing. *P<0.05; **p<0.01; ***p<0.001; ****p<0.0001; ns, not significant. FITC, fluorescein-isothiocyanate.

and increased ZO-1 mRNA expression (figure 2I) in colonic Caco-2 cells.

The anti-obesogenic effects of HSM and H1 are transferable by faecal transplantation

The gut microbiota contributes to the development of diet-induced obesity and associated metabolic disorders.[12–15] Given that HSM and H1 reduced serum endotoxemia and intestinal permeability (figure 2A,B), we examined whether the beneficial effects of HSM and H1 may be mediated by the gut microbiota. Faecal microbiota from HFD-fed or chow-fed mice treated with saline, HSM, fraction H1 or fraction H4 were transplanted into HFD-fed recipients (see online supplementary figure S10A). FMT from HSM-treated, H1-treated or chow-treated mice reduced body weight gain and obesity traits in HFD recipients (see online supplementary figure S10B–G,I). FMT from HSM, H1 or chow groups increased colonic ZO-1 mRNA expression compared with the controls (see online supplementary figure S10H). Furthermore, FMT from HSM, H1 or chow groups reduced adipocyte hypertrophy and CLS lesions (see online supplementary figure S11), as well as signs of NAFLD and NASH in the liver of HFD recipients (see online supplementary figure S12). In contrast, FMT derived from saline-treated or H4-treated, HFD-fed mice failed to reverse obesity traits in HFD-fed recipients (see online supplementary figures S10–12). These results suggest that the gut microbiota mediates the anti-obesogenic effects produced by HSM and H1.

Neomycin abolishes H1's anti-obesogenic effects

To determine whether the anti-obesogenic effects of H1 are dependent on the presence of specific gut bacteria, we treated H1-fed HFD mice with a cocktail of antibiotics, which included

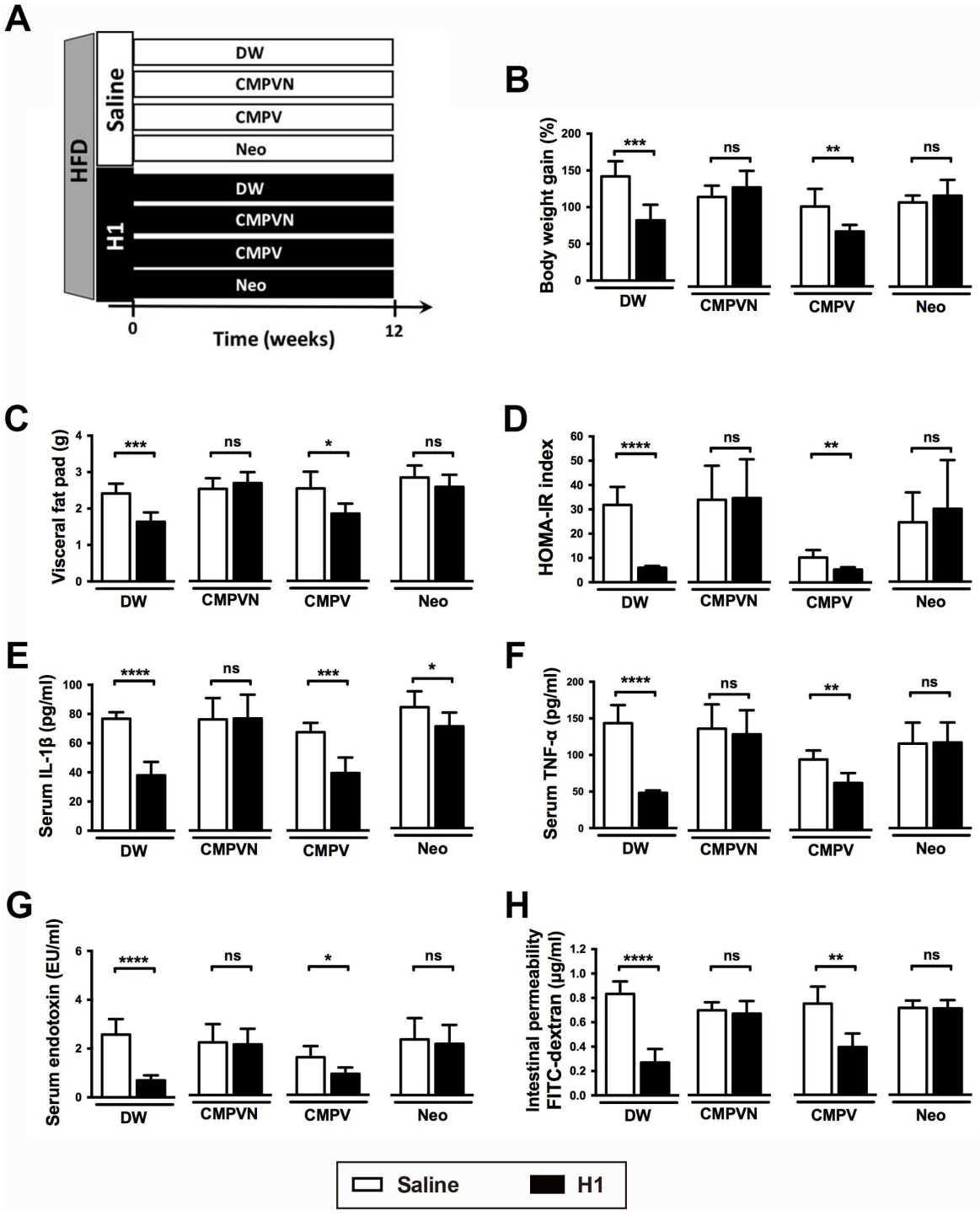

Figure 3 H1 produces anti-obesogenic effects via neomycin-sensitive gut bacteria. (A) Saline-treated or H1-treated high-fat diet (HFD)-fed mice were treated orally with antibiotics in sterile drinking water (DW) for 12 weeks as described in the 'Methods' section. Obesity traits including (B) body weight gain, (C) visceral fat pad weight, (D) homeostatic model assessment-insulin resistance (HOMA-IR) index, (E) serum interleukin (IL)-1β, (F) serum tumour necrosis factor-alpha (TNF-α), (G) serum endotoxin (lipopolysaccharide (LPS)) and (H) intestinal permeability were measured after 12 weeks of treatment. Data are presented as means±SD (n=6 mice/group). Statistical analysis was performed using unpaired Student's t-test between saline and H1 groups, followed by false discovery rate correction for multiple testing. *P<0.05; **p<0.01; ***p<0.001; ****p<0.0001; C, clindamycin; FITC, fluorescein-isothiocyanate; M, metronidazole; P, penicillin; V, vancomycin; N or Neo, neomycin; ns, not significant.

clindamycin (C), metronidazole (M), penicillin (P), vancomycin (V) and neomycin (N) in DW (figure 3A). Compared with the antibiotic-free DW control group in which H1 reduced body weight gain and obesity traits (figure 3B–H and supplementary figures S13–15, DW control group), treatment with the CMPVN antibiotic cocktail abolished H1's anti-obesogenic effects (figure 3B–H and supplementary figures S14 and 15, CMPVN treatment).

To determine whether a single antibiotic from the cocktail may be responsible for these effects, we treated mice with individual antibiotics (see online supplementary figure S13A). Of note, with the exception of serum IL-1β (figure 3E), neomycin consistently

abrogated H1's anti-obesogenic effects (figure 3B–H, supplementary figure S13B–G and supplementary figures S14 and 15, Neo treatment), whereas, with few exceptions, the other single antibiotic treatments failed to block H1's effects (see online supplementary figure S13B-G). Furthermore, H1's anti-obesogenic effects were not affected by an antibiotic cocktail lacking neomycin (figure 3B–H and supplementary figures S14 and 15, CMPV treatment). Neomycin-sensitive gut bacteria may therefore be required for H1's anti-obesogenic effects.

Identification of neomycin-sensitive gut bacteria enriched by H1

We used next-generation 16S rDNA sequencing to analyse the changes produced by H1 in the gut microbiota. Sequencing analysis of caecal samples (figure 4A) produced an average of 117 633±13 834 effective reads per sample that covered rare new phylotypes and broad bacterial diversity (see online supplementary dataset S2). Weighted UniFrac-based principal coordinate analysis revealed distinct clustering of microbiota for each group (see online supplementary figure S16A). Pairwise comparisons using the permutational multivariate analysis of variance (PERMANOVA) test indicated a statistically significant separation between groups ($p<0.05$), except for the comparison between CMPVN and CMPV ($p=0.41$). Analysis of distance matrix revealed that the gut microbiota of neomycin-treated mice clustered with that of HFD-fed mice (see online supplementary figure S16B), revealing similarities between the microbiota of these samples.

We used Metastats analysis to identify the bacteria altered by H1 and neomycin in HFD-fed mice. Operational taxonomic units showing a significant difference between H1 and the other HFD groups were searched against the GenBank sequence database. Overall, 40 bacterial species were significantly altered by H1 in HFD or antibiotics-treated mice (figure 4B,C and supplementary dataset S3). When compared with HFD, H1 altered 16 bacterial species (figure 4B,C; H1 vs HFD, 11 increased species highlighted in red and five reduced species highlighted in green in figure 4C; see also supplementary dataset S3). In H1-treated HFD groups, supplementation with CMPV, neomycin or CMPVN, respectively altered 19, 25 or 27 bacterial species (figure 4B,C; species highlighted in red or green in figure 4C). The chow treatment only affected the levels of nine bacterial species compared with HFD (figure 4B,C; chow vs HFD), indicating that H1 modulates the gut microbiota in a specific manner.

We sought to identify the bacterial species in the H1 group whose abundance was altered by both neomycin and CMPVN. Detailed analysis showed that, among the 40 bacterial species identified, 9 species were modulated in the same direction by both neomycin and CMPVN (figure 4B,C and supplementary dataset S3), including 6 species whose levels were enriched by H1 (*P. goldsteinii*, *Flintibacter butyricus*, *Intestinimonas butyriciproducens*, *Clostridium cocleatum*, *Clostridium viride* and *Anaerotruncus colihominis*) and 3 species whose levels were reduced by H1 (*Pseudomonas aeruginosa*, *Escherichia coli* and *Shewanella algae*). In contrast, three enriched species (*Ruminococcus flavefaciens*, *Butyrivibrio hungatei* and *Ruminococcus bromii*) and three depleted species (*Mucispirillum schaedleri*, *Dorea longicatena* and *Romboutsia timonensis*) were significantly modulated by H1 but reversed by neomycin treatment. Species whose levels were enriched by H1 but reduced by CMPVN included *Ruminococcus gnavus*, *Ochrobactrum anthropic* and *Delftia acidovorans*.

Among the altered species identified, *M. schaedleri*, *D. longicatena*, *R. timonensis*, *E. coli* and *S. algae* represent endotoxin-producing bacteria whose levels increased in obese animals.[33 42 43] Notably, several altered species, including *P. goldsteinii*, *C. cocleatum*, *A. colihominis* and *R. flavefaciens*, were reduced in obese animals and humans.[33 44 45] Our results showed that several bacterial species were altered in the same direction in the HFD group by CMPV, neomycin and CMPVN (figure 4C). Of note, the levels of four species, including *P. goldsteinii*, *I. butyriciproducens*, *C. cocleatum* and *S. algae*, were significantly altered by H1 but reversed by neomycin and CMPVN (figure 4C).

We examined whether obesity-related traits correlated with the levels of neomycin-sensitive gut bacteria enriched by H1. Spearman's correlation analysis showed that the levels of these bacteria negatively correlated with obesity traits (figure 4D). Notably, among these bacteria, *P. goldsteinii* was highly enriched by H1 treatment (figure 4B,C and supplementary dataset S3) and this species negatively correlated with all obesity traits (figure 4D and supplementary dataset S4). The levels of other H1-modulated neomycin-sensitive bacteria were also associated with *P. goldsteinii* levels (see online supplementary figure S17). These results suggest that *P. goldsteinii* and the neomycin-sensitive gut microbiota might mediate the anti-obesogenic effects of H1.

Ex vivo neomycin treatment abolishes the anti-obesogenic effects of H1

To eliminate potential side effects produced by antibiotics on the host, we treated faecal microbiota with antibiotics ex vivo prior to FMT (ex-FMT; figure 5A). Faecal microbiota specimens collected daily from H1-treated HFD-fed mice were incubated with antibiotics or saline, followed by washing steps and oral administration into HFD-fed recipients (figure 5A). As expected, the HFD-induced obesity traits of HFD recipients were significantly reduced by ex-FMT from H1-treated mice (figure 5B–H, H1 vs HFD), and these effects were abolished by ex-FMT from neomycin-treated or CMPVN-treated animals (figure 5B–H). In contrast, ex-FMT from CMPV-treated H1-faecal microbiota prevented obesity traits in HFD animals (figure 5B–H, CMPV).

P. goldsteinii levels negatively correlate with obesity traits in ex vivo FMT

We analysed the microbiota of ex-FMT mice to identify bacteria that were enriched by H1 but reduced by neomycin or CMPVN in donor and recipient mice. In the donor group, when compared with HFD, levels of eight bacterial species were significantly altered by H1 but reversed by neomycin and CMPVN (figure 6A,B and supplementary dataset S5). These bacteria included six species whose levels were enriched by H1 (*P. goldsteinii*, *Clostridium perfringens*, *C. viride*, *Adlercreutzia equolifaciens*, *Paenibacillus glucanolyticus* and *Bradyrhizobium japonicum*) and two species whose levels were reduced by H1 (*Lactobacillus johnsonii* and *Lactobacillus reuteri*; figure 6A,B and supplementary dataset S5). Among these bacteria, *P. goldsteinii* was significantly enriched in H1 donor mice but considerably reduced by neomycin or CMPVN (figure 6A,B). Accordingly, *P. goldsteinii* was also enriched in H1-recipient mice but reduced in CMPVN-recipient mice (figure 6C,D and supplementary dataset S6). Based on quantitative PCR, we observed that the absolute *P. goldsteinii* count increased following H1 treatment but the bacterial count was considerably reduced by neomycin or CMPVN in both donor and recipient mice (figure 6E). Notably,

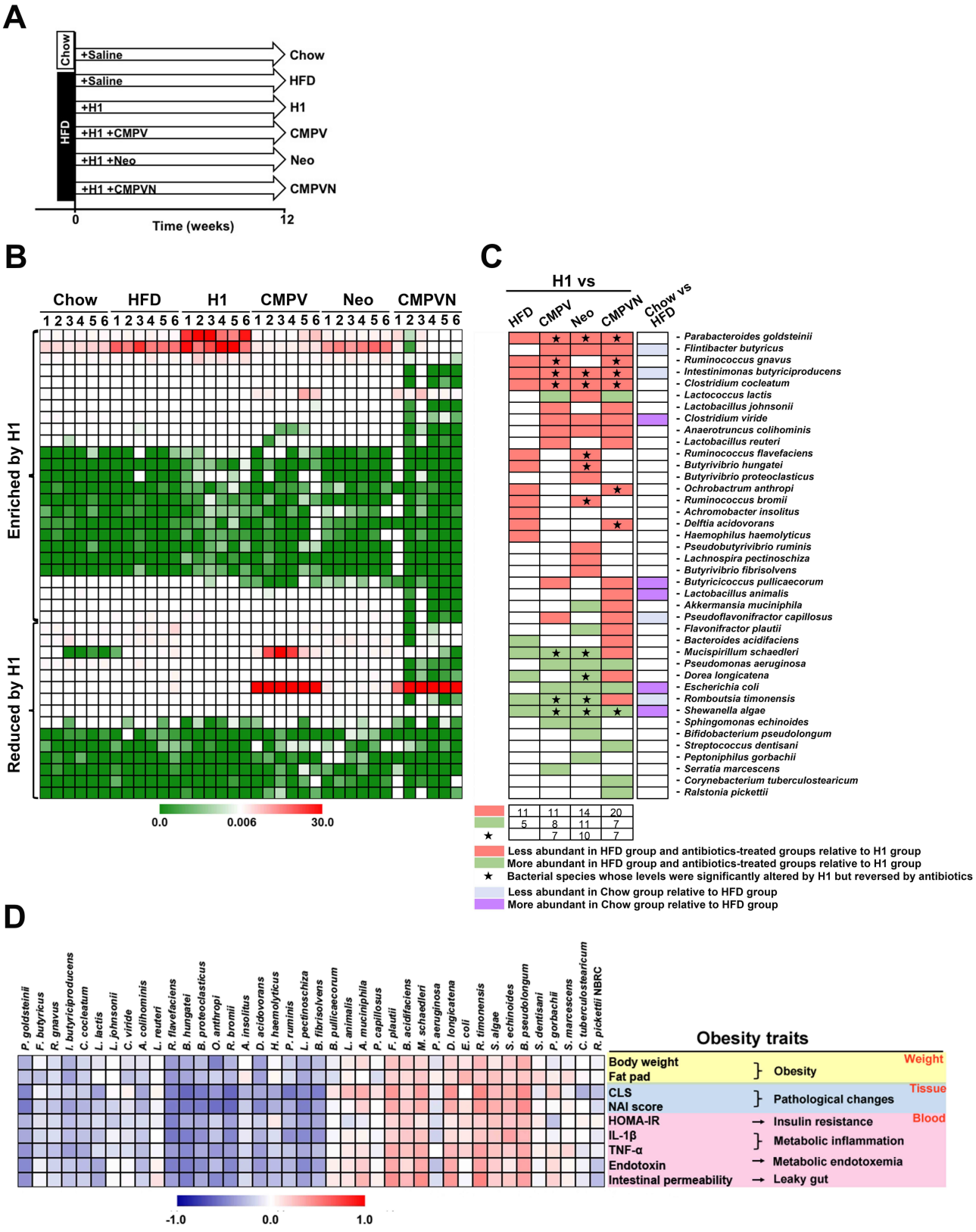

Figure 4 H1 enriches a population of neomycin-sensitive gut bacteria that negatively correlates with obesity traits. (A) Mice were treated for 12 weeks as indicated. (B) Heatmap showing the levels of 40 bacterial species significantly altered by high-fat diet (HFD) or antibiotics in comparison with the H1 group based on Metastats analysis. (C) Bacterial species from panel B and changes induced by the treatments indicated. Green and red entries indicate species that were respectively more and less abundant in the HFD group and antibiotics-treated groups relative to H1. Purple and blue entries indicate species that were respectively more and less abundant in the chow group relative to the HFD group. Black stars indicate bacterial species whose levels were significantly altered by H1 but reversed by antibiotics. (D) Spearman's correlation analysis between the 40 identified bacterial species and obesity traits. False discovery rate correction for multiple testing was used. CLS, crown-like structure; HOMA-IR, homeostatic model assessment-insulin resistance; IL, interleukin; NAI, non-alcoholic steatohepatitis activity index; TNF-α, tumour necrosis factor-alpha.

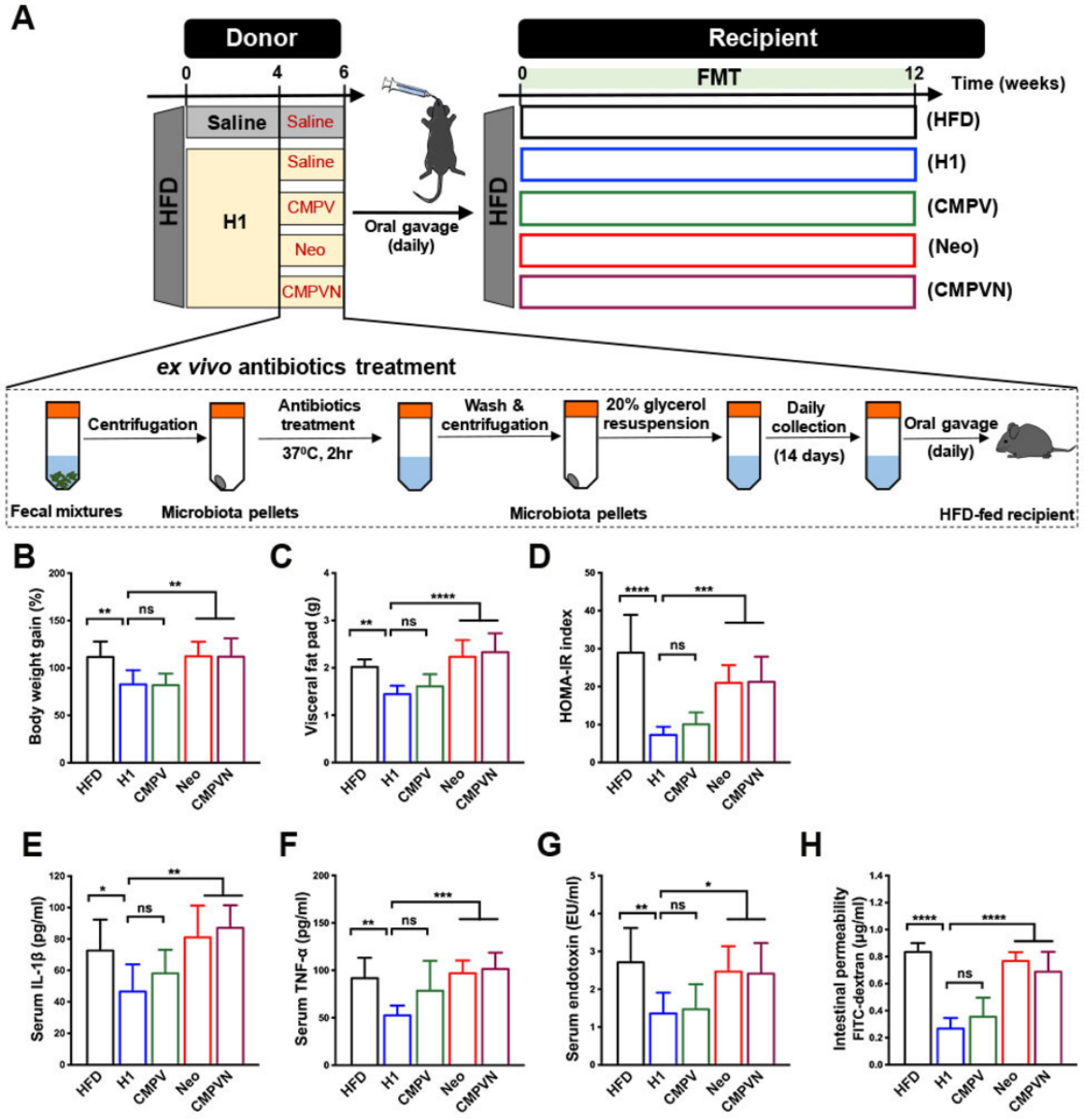

Figure 5 Ex vivo neomycin treatment abolishes the anti-obesogenic effects of faecal microbiota transplantation (FMT) from H1-treated mice. (A) Diagram of ex vivo antibiotics treatment of faecal bacteria before FMT (ex-FMT). High-fat diet (HFD)-fed donor mice were treated daily with saline or H1 by oral gavage for 6 weeks. H1-treated faeces samples were collected daily from week 4 to 6, followed by a series of steps for ex vivo antibiotics treatment (CMPV, Neo, CMPVN or saline; see the enlarged rectangle). Faecal microbiota from saline-treated HFD-fed mice was used as a negative control. Faecal microbiota samples collected for 2 weeks from each donor mice were pooled and an equal volume was transferred to HFD-fed mice by oral gavage for 12 weeks. Obesity traits measured in recipients after 12 weeks included (B) body weight gain, (C) visceral fat pad weight, (D) homeostatic model assessment-insulin resistance (HOMA-IR) index, (E) serum interleukin (IL)-1β, (F) serum tumour necrosis factor-alpha (TNF-α), (G) serum endotoxin and (**H**) intestinal permeability. Data are presented as means±SD from two independent experiments (n=9). Data were analysed using one-way analysis of variance followed by Bonferroni's post hoc test and false discovery rate correction for multiple testing. *P<0.05; **p<0.01; ***p<0.001; ****p<0.0001; ns, not significant; FITC, fluorescein-isothiocyanate.

both the absolute count (copy number) and relative level of *P. goldsteinii* were negatively associated with obesity traits (figure 6F).

P. goldsteinii prevents diet-induced obesity and metabolic disorders

In order to confirm that *P. goldsteinii* had colonised mice in FMT experiments, we examined the levels of *P. goldsteinii* in caecal microbiota of HFD-fed mice treated with saline, HSM or H1 as well as in their recipients. Levels of *P. goldsteinii* between paired donors and recipients were similar (see online supplementary figure S18A,B), indicating an efficient transfer of *P. goldsteinii* during FMT. Moreover, colonisation was observed in HFD-fed mice treated with neomycin for 8 weeks and which received a single oral gavage of *P. goldsteinii* (see online supplementary figure S18C).

These results prompted us to examine whether *P. goldsteinii* produces anti-obesogenic effects in HFD-fed mice. We treated HFD-fed mice daily with a commercial strain of *P. goldsteinii* or saline for 8 weeks (figure 7A). *P. goldsteinii* treatment

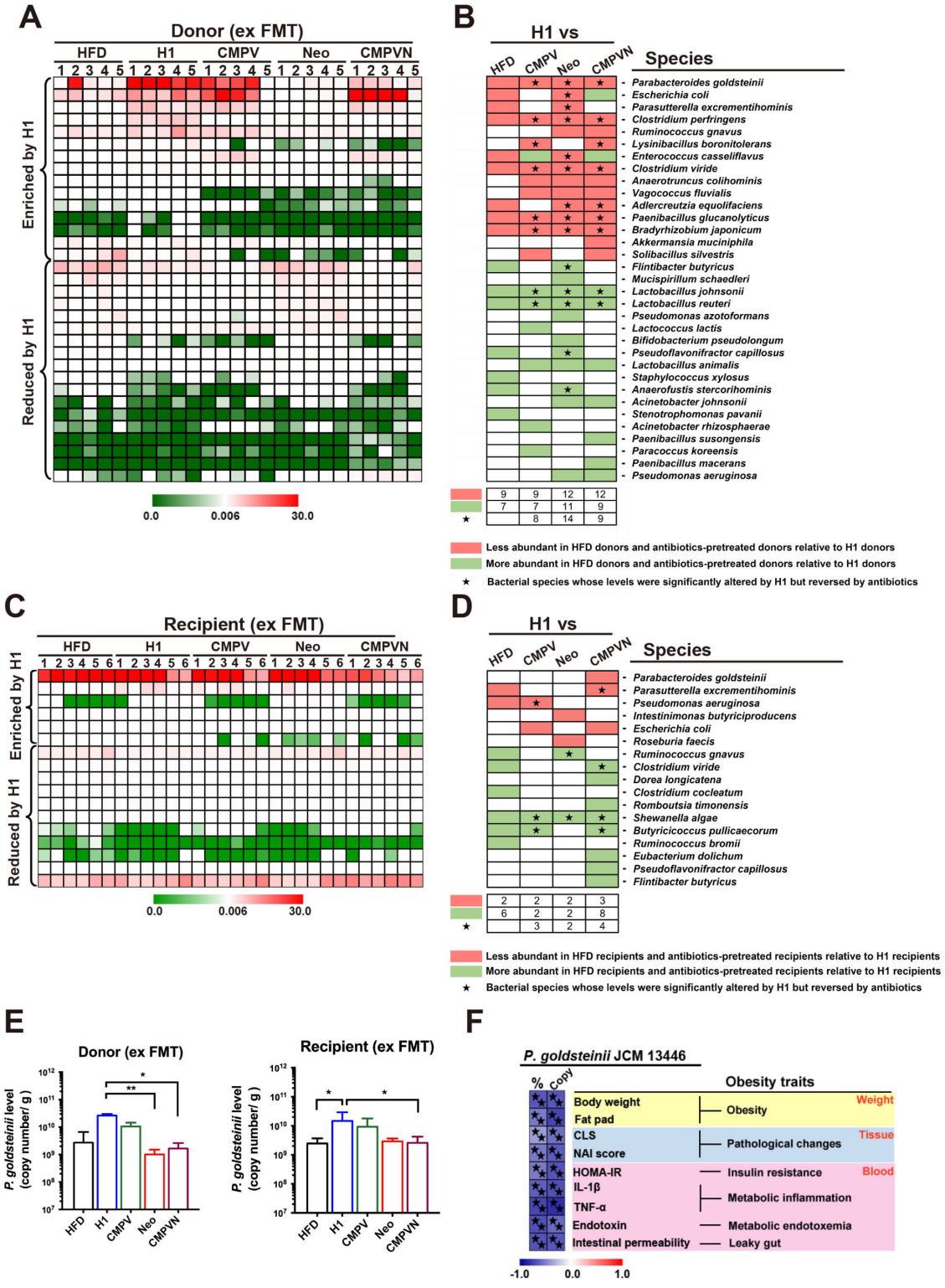

Figure 6 *Parabacteroides goldsteinii* is enriched in ex vivo faecal microbiota transplantation (ex FMT) H1 donor and recipient mice and negatively correlates with obesity traits. The ex-FMT experiments are depicted in figure 5A. (A) Heatmap abundance and (B) bacterial species information showing 33 bacterial species significantly altered by H1 in donor groups based on Metastats analysis. (C) Heatmap abundance and (D) bacterial species information showing 17 bacterial species significantly altered by H1 in recipient groups based on Metastats analysis. In panels (B) and (D), green and red entries indicate species that were respectively more and less abundant in the high-fat diet (HFD) group and ex vivo antibiotics-treated groups relative to H1. Black stars indicate bacterial species whose levels were significantly altered by H1 but reversed by antibiotics. (E) Absolute quantification (copy number) of *P. goldsteinii* in ex-FMT donor groups (left panel) and recipient groups (right panel). Data are presented as medians±IQR (n=5 and n=6 for donor and recipient groups, respectively). (F) Spearman's correlation analysis of relative abundance (%) and absolute count (copy) of *P. goldsteinii* and obesity traits. In this panel, black stars indicate statistically significant difference based on Spearman's correlation analysis and false discovery rate correction (<5%). *P<0.05; **p<0.01; CLS, crown-like structures; HOMA-IR, homeostatic model assessment-insulin resistance; IL, interleukin; NAI, non-alcoholic steatohepatitis activity index; TNF-α, tumour necrosis factor-alpha.

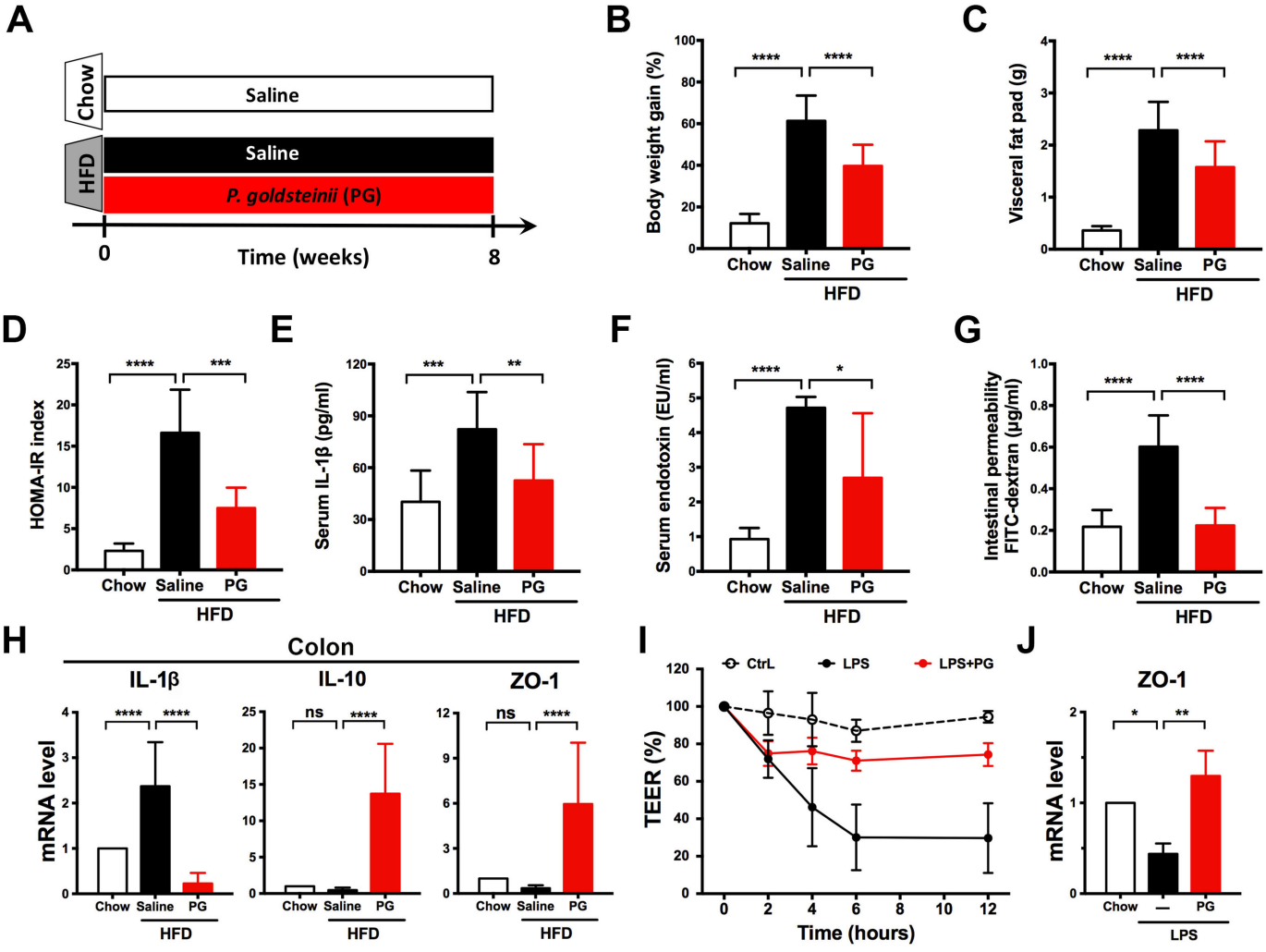

Figure 7 *Parabacteroidesgoldsteinii* (PG) reduces diet-induced obesity and metabolic disorders. (A) Chow-fed mice and high-fat diet (HFD)-fed mice were treated daily with saline or PG (4×10^7 colony-forming units) by oral gavage for 8 weeks. Obesity traits including (B) body weight gain, (C) visceral fat pad, (D) homeostatic model assessment-insulin resistance (HOMA-IR) index, (E) serum interleukin (IL)-1β, (F) serum endotoxin and (G) intestinal permeability were measured after 8 weeks of treatment. (H) IL-1β, IL-10 and ZO-1 expression in proximal colon was examined using quantitative real-time PCR (qRT-PCR). Expression was normalised to glyceraldehyde 3-phosphate dehydrogenase and expressed as relative fold changes compared with the chow group. (I) Caco-2 cell permeability was monitored in vitro using the transepithelial electrical resistance (TEER) assay. (J) Zonula occludens-1 (ZO-1) expression in Caco-2 cell monolayers was examined using qRT-PCR. Expression was normalised to 18S rRNA and expressed as relative fold changes compared with the vehicle control (CtrL). Data are presented as means±SD of three independent experiments. n=16–19 mice for panels B,C; n=6 for panels D, F, G; n=11 for panels E, H; n=3 for panels I, J. Data were analysed using one-way analysis of variance followed by Bonferroni's post hoc test and false discovery rate correction for multiple testing. *P<0.05; **p<0.01; ***p<0.001; ****p<0.0001; ns, not significant.

significantly reduced body weight gain (20%–35% reduction), visceral fat, HOMA-IR index, serum levels of IL-1β and endotoxin and intestinal permeability (figure 7B–G), and these results were accompanied by reduced IL-1β mRNA expression and increased IL-10 and ZO-1 mRNA expression in colon tissues (figure 7H). *P. goldsteinii* treatment also effectively reduced cell monolayer disruption and restored tight junction ZO-1 expression in LPS-treated Caco-2 cell monolayers (figure 7I,J). In chow-fed mice, *P. goldsteinii* treatment reduced body weight, but did not affect other obesity-related traits (see online supplementary figure S19). *P. goldsteinii* treatment reduced adipocyte hypertrophy and CLS lesions in adipose tissues of HFD-fed mice (see online supplementary figure S20). *P. goldsteinii* significantly increased UCP1 mRNA and protein expression in BATs and iWATs (see online supplementary figure S21), suggesting that the bacterium may induce thermogenesis. Furthermore, *P. goldsteinii* reduced signs of NAFLD and NASH in HFD-fed mice (see online supplementary figure S22), and normalised gene expression involved in lipid transport, lipogenesis and β-oxidation in the liver (see online supplementary figure S23, no statistically significant effect was noted for SREBP1c). Notably, administration of either heat-killed or pasteurised *P. goldsteinii* failed to reduce body weight or visceral fat accumulation (see online supplementary figure S24), indicating that live bacteria are required to induce anti-obesogenic effects. Finally, *P. goldsteinii* treatment did not affect liver or kidney functions in chow-fed or HFD-fed mice (see online supplementary table S2). *P. goldsteinii* therefore induces anti-obesogenic, anti-inflammatory and antidiabetic effects in obese animals.

DISCUSSION

Although previous studies have shown that the medicinal fungus *O. sinensis* may lower blood glucose and lipid levels in type 2 diabetes in mice,[46–49] the possibility that this fungus may modulate the gut microbiota and reduce body weight in animals had not been examined. Our study shows that a water extract of the *H. sinensis* fungus (ie, HSM) and a fraction containing high-molecular weight polysaccharides (ie, fraction H1) reduce diet-induced obesity and metabolic disorders by modulating gut microbiota composition, improving intestinal integrity and inducing thermogenesis. H1 treatment reverses HFD-induced gut dysbiosis and increases the level of *P. goldsteinii* and other neomycin-sensitive bacteria. Such changes in the composition of the gut microbiota in turn improve HFD-induced intestinal integrity and insulin sensitivity, and reduce metabolic endotoxemia, inflammation, fat deposition, adipose tissue pathology and the development of fatty liver disease (figure 8). We also observed that H1 reduced LPS-induced cellular permeability in human intestinal Caco-2 cells (figure 2H,I), indicating that

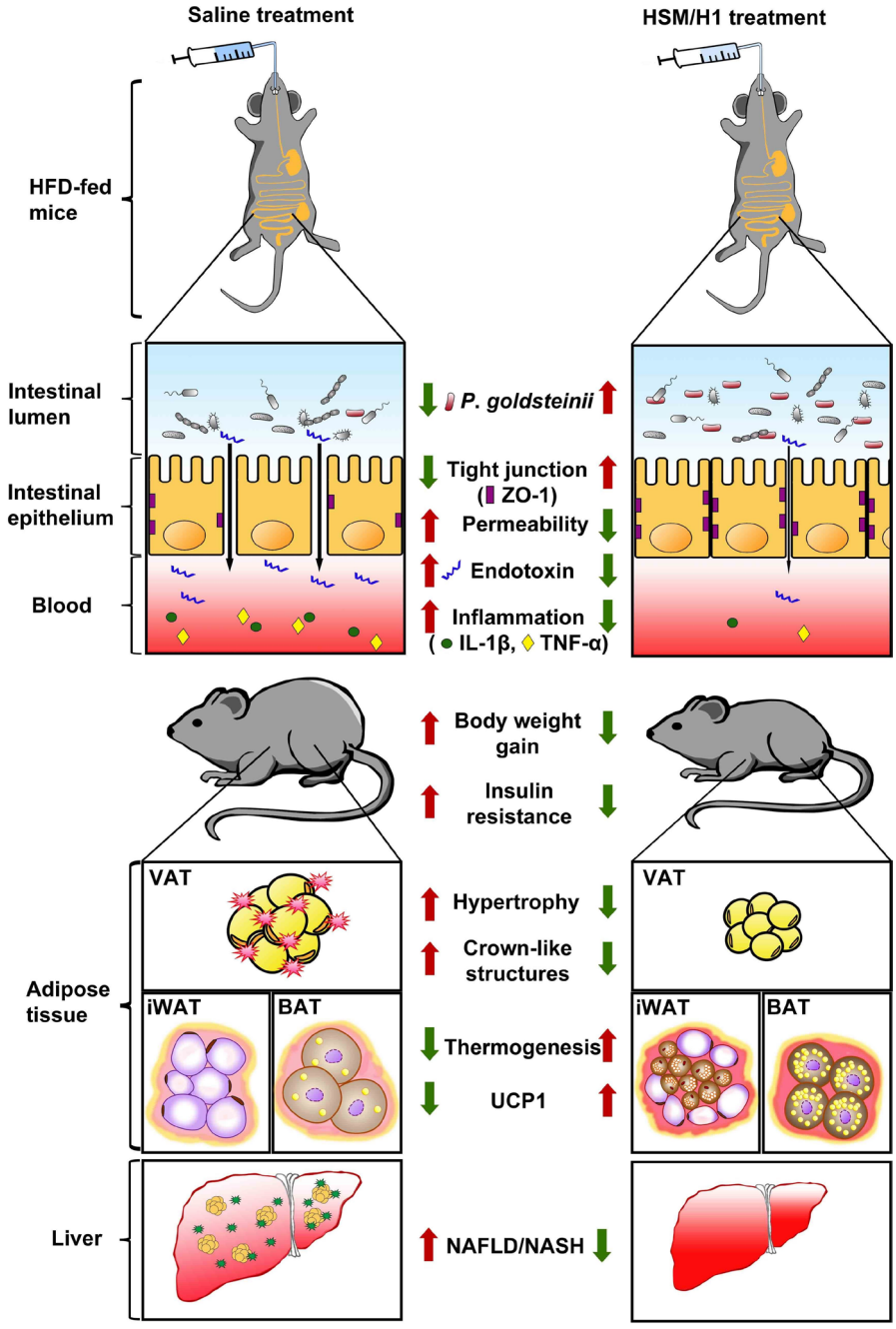

Figure 8 Proposed model for the anti-obesogenic effects of *Hirsutella sinensis* mycelium (HSM) and H1 in high-fat diet (HFD)-fed mice. Treatment with HSM or H1 produces many beneficial changes on HFD-fed mice, including increasing *Parabacteroides goldsteinii* levels, tight junction expression and thermogenesis, while reducing gut permeability, blood endotoxin levels, inflammation and body weight. HSM and H1 also reduce insulin resistance, adipocyte hypertrophy, crown-like structures and signs of fatty liver disease (non-alcoholic fatty liver disease (NAFLD)/non-alcoholic steatohepatitis (NASH)). BAT, brown adipose tissue; IL, interleukin; iWAT, inguinal white adipose tissue; TNF-α, tumour necrosis factor-alpha; UCP1, uncoupling protein 1; VAT, visceral adipose tissue; ZO-1, zonula occludens-1.

H1 may improve intestinal integrity independently of the gut microbiota.

Our results show that *P. goldsteinii* treatment reduces obesity and metabolic disorders in HFD-fed mice, in addition to maintaining intestinal integrity, inducing thermogenesis and reducing endotoxemia and inflammation (figure 7A–H and supplementary figure S21). Intriguingly, a recent study showed that zwitterionic capsular polysaccharides derived from various commensal gut bacteria produce anti-inflammatory effects by inducing regulatory T cells.[50] Our observations that *P. goldsteinii* treatment induces expression of IL-10 (figure 7H) and helps maintain intestinal integrity (figure 7G,I,J) support the possibility that the bacterium may preserve intestinal homeostasis and improve gut barrier functions in vivo.

Our previous study showed that polysaccharides isolated from a water extract of the medicinal fungus *G. lucidum* also produce anti-obesogenic effects in HFD-fed mice.[33] Compared with the *G. lucidum* polysaccharides identified earlier, the monosaccharide composition of H1 identified here shows a higher content of mannose, galactose, N-galactosamine, N-glucosamine, rhamnose and fucose (see online supplementary table S3). Cordyceps polysaccharides have been found to contain β-glucans, heteroglycans and cordyglucans,[29] but the molecular structure and functional motifs of H1's high-molecular weight polysaccharides remain to be determined. While polysaccharides are predominantly enriched during water-based extraction procedures such as the one used to prepare the H1 fraction, we could not exclude the possibility that other bioactive molecules present in the extract may also contribute to the anti-obesogenic effects of this fraction. Moreover, we previously observed that *P. goldsteinii* levels in the gut microbiota of HFD-fed mice increased following treatment with *G. lucidum* polysaccharides,[33] suggesting that this commensal bacterial species may mediate the anti-obesogenic effects of polysaccharides isolated from various medicinal fungi.

The breakdown of polysaccharides and dietary fibre in mammals is mainly performed by intestinal bacteria, such as *Bacteroides thetaiotaomicron* and *Bacteroides fragilis*,[51–54] resulting in modulation of nutrient absorption and energy levels. HSM and H1 treatment did not alter energy intake, stool fat content or intestinal SCFA production (see online supplementary figures S2 and S3), indicating that the anti-obesity effects of H1 are not due to reduction of appetite, modulation of nutrient absorption or enhanced production of SCFAs. The reduction of *P. goldsteinii* levels by HFD and enrichment of this bacterial species by fungal polysaccharides indicate that the gut microbiota of polysaccharide-treated mice may contain higher levels of bacteria that preferentially metabolise polysaccharides. Enrichment of *P. goldsteinii* by H1 is also associated with reduced levels of bacterial species that are positively associated with obesity, such as *M. schaedleri* and *S. algae* (figure 4C).[33 42 43 55]

We observed that the anti-obesogenic effects of H1 are dependent on neomycin-sensitive gut bacteria (figures 3–6). The presence of a population of neomycin-sensitive gut bacteria and its association with obesity-related traits (figure 4D) suggests a potential beneficial interplay between these bacteria and energy regulation and metabolism. In the present study, H1 treatment did not affect the level of known commensal bacteria that possess anti-obesogenic properties, such as *A. muciniphila*,[23 56] *L. reuteri*[57] or *L. johnsonii*[58] (figure 4C). Further study of the functional gut microbiota and examination of their mechanism of action will be required to identify new strategies to prevent and treat obesity and related metabolic disorders.[59]

Several medicinal fungi and plants produce beneficial effects on obesity and diabetes by modulating a variety of physiological pathways in the body.[28] In comparison to fractions H2 to H4, which produced small effects on a limited number of obesity traits (see for instance figure 1E and supplementary figure S4), HSM and fraction H1 produced consistent anti-obesogenic, antidiabetic and anti-inflammatory effects on all major obesity traits examined in HFD-fed mice, including HOMA-IR index (figure 1F), inflammation (figure 1G,H), metabolic endotoxemia (figure 2A) and intestinal permeability (figure 2B). Furthermore, besides reducing gene expression involved in lipogenic pathways in adipose and hepatic tissues (see online supplementary figure S4B,C), treatment with HSM and H1 significantly induced β-oxidation in the liver (see online supplementary figure S4C, Acsl3). These results suggest that HSM and H1 may target specific metabolic and immunological pathways to normalise inflammatory markers and the metabolic profile of obese mice.

In conclusion, our results indicate that a water extract of a medicinal fungus and its high-molecular weight polysaccharide fraction reduce obesity, inflammation and diabetes-related symptoms by modulating the composition of the gut microbiota. Our findings show that both HSM and its high-molecular weight polysaccharides may be used as prebiotics—while the intestinal bacterium *P. goldsteinii* may be used as a probiotic—to prevent and treat obesity and the associated metabolic disorders.

Author affiliations
[1]Department of Medical Biotechnology and Laboratory Science, College of Medicine, Chang Gung University, Gueishan, Taiwan
[2]Graduate Institute of Biomedical Sciences, College of Medicine, Chang Gung University, Gueishan, Taiwan
[3]Center for Molecular and Clinical Immunology, Chang Gung University, Gueishan, Taiwan
[4]Microbiota Research Center, Chang Gung University, Gueishan, Taiwan
[5]Chang Gung Immunology Consortium, Linkou Chang Gung Memorial Hospital, Gueishan, Taiwan
[6]Research Center for Emerging Viral Infections, Chang Gung University, Gueishan, Taiwan
[7]Chang Gung Biotechnology Corporation, Taipei, Taiwan
[8]Biochemical Engineering Research Center, Ming Chi University of Technology, Taishan, Taiwan
[9]Department of Biomedical Sciences, University of the Pacific, Arthur Dugoni School of Dentistry, San Francisco, California, USA
[10]Department of Respiratory Therapy, Fu Jen Catholic University, Xinzhuang, Taiwan
[11]Laboratory of Cellular Physiology and Immunology, Rockefeller University, New York, USA
[12]Department of Laboratory Medicine, Linkou Chang Gung Memorial Hospital, Gueishan, Taiwan
[13]Research Center for Chinese Herbal Medicine, College of Human Ecology, Chang Gung University of Science and Technology, Gueishan, Taiwan
[14]Research Center for Food and Cosmetic Safety, College of Human Ecology, Chang Gung University of Science and Technology, Gueishan, Taiwan

Acknowledgements The authors would like to thank Dr Yu-Lun Kuo (Biotools) for the kind assistance with microbiota sequencing and analysis as well as Dr Yueh-Hsia Chiu (Chang Gung University) regarding the statistical analysis. The authors would also like to thank Drs Yu-Huan Tsai (Chang Gung University) and Julieta Schachter (Universidade Federal de Rio de Janeiro, Brazil) for their comments on the manuscript.

Contributors T-RW, C-SL and C-JC conceived the project, contributed to experimental design, performed experiments, interpreted the results, prepared the figures and wrote the manuscript; T-LL performed experiments and interpreted the results; JDY and H-CL conceived and supervised the project, interpreted the results and wrote the manuscript; JM, DMO and C-CL interpreted the results and wrote the manuscript; Y-FK provided the HSM extract and polysaccharides fractions; all authors discussed the results and approved the manuscript.

Funding The authors' work is supported by the Primordia Institute of New Sciences and Medicine; the Research Center for Emerging Viral Infections (Chang Gung University); the Featured Areas Research Center Program, which is part of the Higher Education Sprout Project of the Ministry of Education of Taiwan; by grants MOST105-2320-B-182-032-MY3, MOST105-2320-B-030-004, MOST103-2321-B-182-014-MY3 and MOST107-3017-F-182-001 from the Ministry of Science and Technology of Taiwan; and by grants BMRPA04, CMRPD1E0073, CMRPD1F0123, CORPD1F0011-3, QZRPD142 and QZRPD146 from Chang Gung Memorial Hospital.

Competing interests Y-FK is President of Chang Gung Biotechnology Corporation. JDY is Chairman of the Board of Chang Gung Biotechnology Corporation. The authors own patents related to the preparation and use of medicinal fungi and probiotics.

Patient consent Not required.

Ethics approval This study was approved by Chang Gung University's Institutional Animal Care and Use Committee (Document No. CGU11-117). Experiments were performed in accordance with the guidelines.

Provenance and peer review Not commissioned; externally peer reviewed.

REFERENCES

1 Caballero B. The global epidemic of obesity: an overview. *Epidemiol Rev* 2007;29:1–5.
2 Haslam DW, James WP. Obesity. *Lancet* 2005;366:1197–209.
3 World Health Organization. Obesity and overweight. 2018 http://www.who.int/mediacentre/factsheets/fs311/en/.
4 Visscher TL, Seidell JC. The public health impact of obesity. *Annu Rev Public Health* 2001;22:355–75.
5 Turnbaugh PJ, Ley RE, Mahowald MA, *et al*. An obesity-associated gut microbiome with increased capacity for energy harvest. *Nature* 2006;444:1027–131.
6 Cani PD, Bibiloni R, Knauf C, *et al*. Changes in gut microbiota control metabolic endotoxemia-induced inflammation in high-fat diet-induced obesity and diabetes in mice. *Diabetes* 2008;57:1470–81.
7 Cani PD, Possemiers S, Van de Wiele T, *et al*. Changes in gut microbiota control inflammation in obese mice through a mechanism involving GLP-2-driven improvement of gut permeability. *Gut* 2009;58:1091–103.
8 Cani PD, Amar J, Iglesias MA, *et al*. Metabolic endotoxemia initiates obesity and insulin resistance. *Diabetes* 2007;56:1761–72.
9 Hotamisligil GS. Inflammation and metabolic disorders. *Nature* 2006;444:860–7.
10 Kennedy A, Martinez K, Chuang CC, *et al*. Saturated fatty acid-mediated inflammation and insulin resistance in adipose tissue: mechanisms of action and implications. *J Nutr* 2009;139:1–4.
11 Morris DL, Cho KW, Delproposto JL, *et al*. Adipose tissue macrophages function as antigen-presenting cells and regulate adipose tissue CD4+ T cells in mice. *Diabetes* 2013;62:2762–72.
12 Ridaura VK, Faith JJ, Rey FE, *et al*. Gut microbiota from twins discordant for obesity modulate metabolism in mice. *Science* 2013;341:1241214.
13 Dethlefsen L, McFall-Ngai M, Relman DA. An ecological and evolutionary perspective on human-microbe mutualism and disease. *Nature* 2007;449:811–8.
14 Yoshimoto S, Loo TM, Atarashi K, *et al*. Obesity-induced gut microbial metabolite promotes liver cancer through senescence secretome. *Nature* 2013;499:97–101.
15 Hersoug LG, Møller P, Loft S. Gut microbiota-derived lipopolysaccharide uptake and trafficking to adipose tissue: implications for inflammation and obesity. *Obes Rev* 2016;17:297–312.
16 Aguirre M, Venema K. The art of targeting gut microbiota for tackling human obesity. *Genes Nutr* 2015;10:472.
17 Anand G, Zarrinpar A, Loomba R. Targeting Dysbiosis for the Treatment of Liver Disease. *Semin Liver Dis* 2016;36:037–47.
18 Delzenne NM, Cani PD, Everard A, *et al*. Gut microorganisms as promising targets for the management of type 2 diabetes. *Diabetologia* 2015;58:2206–17.
19 Scott KP, Antoine JM, Midtvedt T, *et al*. Manipulating the gut microbiota to maintain health and treat disease. *Microb Ecol Health Dis* 2015;26:25877.
20 Sonnenburg JL, Bäckhed F. Diet-microbiota interactions as moderators of human metabolism. *Nature* 2016;535:56–64.
21 Delzenne NM, Neyrinck AM, Bäckhed F, *et al*. Targeting gut microbiota in obesity: effects of prebiotics and probiotics. *Nat Rev Endocrinol* 2011;7:639.46.
22 Everard A, Lazarevic V, Derrien M, *et al*. Responses of gut microbiota and glucose and lipid metabolism to prebiotics in genetic obese and diet-induced leptin-resistant mice. *Diabetes* 2011;60:2775–86.
23 Everard A, Belzer C, Geurts L, *et al*. Cross-talk between *Akkermansia muciniphila* and intestinal epithelium controls diet-induced obesity. *Proc Natl Acad Sci U S A* 2013;110:9066–71.
24 Wang J, Tang H, Zhang C, *et al*. Modulation of gut microbiota during probiotic-mediated attenuation of metabolic syndrome in high fat diet-fed mice. *Isme J* 2015;9:1–15.
25 De Vadder F, Kovatcheva-Datchary P, Goncalves D, *et al*. Microbiota-generated metabolites promote metabolic benefits via gut-brain neural circuits. *Cell* 2014;156:84–96.
26 Nakamura YK, Omaye ST. Metabolic diseases and pro- and prebiotics: Mechanistic insights. *Nutr Metab* 2012;9:60.
27 Parnell JA, Reimer RA. Prebiotic fiber modulation of the gut microbiota improves risk factors for obesity and the metabolic syndrome. *Gut Microbes* 2012;3:29–34.
28 Martel J, Ojcius DM, Chang CJ, *et al*. Anti-obesogenic and antidiabetic effects of plants and mushrooms. *Nat Rev Endocrinol* 2017;13:149–60.
29 El Enshasy HA, Hatti-Kaul R. Mushroom immunomodulators: unique molecules with unlimited applications. *Trends Biotechnol* 2013;31:668–77.
30 Wasser SP. Medicinal mushroom science: Current perspectives, advances, evidences, and challenges. *Biomed J* 2014;37:345–56.
31 Martel J, Ko YF, Ojcius DM, *et al*. Immunomodulatory Properties of Plants and Mushrooms. *Trends Pharmacol Sci* 2017;38:967–81.
32 Martel J, Ko YF, Liau JC, *et al*. Myths and Realities Surrounding the Mysterious Caterpillar Fungus. *Trends Biotechnol* 2017;35:1017–21.
33 Chang CJ, Lin CS, Lu CC, Cc L, *et al*. *Ganoderma lucidum* reduces obesity in mice by modulating the composition of the gut microbiota. *Nat Commun* 2015;6:7489.
34 Lo HC, Hsieh C, Lin FY, *et al*. A Systematic Review of the Mysterious Caterpillar Fungus *Ophiocordyceps sinensis* in Dong-ChongXiaCao (Dōng Chóng Xià Cǎo) and Related Bioactive Ingredients. *J Tradit Complement Med* 2013;3:16–32.
35 Zhu ZY, Liu XC, Fang XN, *et al*. Structural characterization and anti-tumor activity of polysaccharide produced by *Hirsutella sinensis*. *Int J Biol Macromol* 2016;82:959–66.
36 Ko YF, Liau JC, Lee CS, *et al*. Isolation, Culture and Characterization of *Hirsutella sinensis* Mycelium from Caterpillar Fungus Fruiting Body. *PLoS One* 2017;12:e0168734.
37 Wang CY, Liao JK. A mouse model of diet-induced obesity and insulin resistance. *Methods Mol Biol* 2012;821:421–33.
38 White JR, Nagarajan N, Pop M. Statistical methods for detecting differentially abundant features in clinical metagenomic samples. *PLoS Comput Biol* 2009;5:e1000352.
39 Benjamini Y, Krieger AM, Yekutieli D. Adaptive linear step-up procedures that control the false discovery rate. *Biometrika* 2006;93:491–507.
40 Shabalina IG, Petrovic N, de Jong JM, *et al*. UCP1 in brite/beige adipose tissue mitochondria is functionally thermogenic. *Cell Rep* 2013;5:1196–203.
41 Kim KA, Gu W, Lee IA, *et al*. High fat diet-induced gut microbiota exacerbates inflammation and obesity in mice via the TLR4 signaling pathway. *PLoS One* 2012;7:e47713.
42 Johnson-Henry KC, Donato KA, Shen-Tu G, *et al*. *Lactobacillus rhamnosus* strain GG prevents enterohemorrhagic *Escherichia coli* O157:H7-induced changes in epithelial barrier function. *Infect Immun* 2008;76:1340–8.
43 Chiu CM, Huang WC, Weng SL, *et al*. Systematic analysis of the association between gut flora and obesity through high-throughput sequencing and bioinformatics approaches. *Biomed Res Int* 2014;2014:1–10.
44 Lee H, Ko G. Effect of metformin on metabolic improvement and gut microbiota. *Appl Environ Microbiol* 2014;80:5935–43.
45 Clarke SF, Murphy EF, Nilaweera K, *et al*. The gut microbiota and its relationship to diet and obesity: new insights. *Gut Microbes* 2012;3:186–202.
46 Kan WC, Wang HY, Chien CC, *et al*. Effects of Extract from Solid-State Fermented *Cordyceps sinensis* on Type 2 Diabetes Mellitus. *Evid Based Complement Alternat Med* 2012;2012:1–10.
47 Koh JH, Kim JM, Chang UJ, *et al*. Hypocholesterolemic effect of hot-water extract from mycelia of *Cordyceps sinensis*. *Biol Pharm Bull* 2003;26:84–7.
48 Li SP, Zhang GH, Zeng Q, *et al*. Hypoglycemic activity of polysaccharide, with antioxidation, isolated from cultured Cordyceps mycelia. *Phytomedicine* 2006;13:428–33.
49 Shi B, Wang Z, Jin H, *et al*. Immunoregulatory *Cordyceps sinensis* increases regulatory T cells to Th17 cell ratio and delays diabetes in NOD mice. *Int Immunopharmacol* 2009;9:582–6.
50 Neff CP, Rhodes ME, Arnolds KL, *et al*. Diverse Intestinal Bacteria Contain Putative Zwitterionic Capsular Polysaccharides with Anti-inflammatory Properties. *Cell Host Microbe* 2016;20:535–47.
51 Krajmalnik-Brown R, Ilhan ZE, Kang DW, *et al*. Effects of gut microbes on nutrient absorption and energy regulation. *Nutr Clin Pract* 2012;27:201–14.
52 Ravcheev DA, Godzik A, Osterman AL, *et al*. Polysaccharides utilization in human gut bacterium *Bacteroides thetaiotaomicron*: comparative genomics reconstruction of metabolic and regulatory networks. *BMC Genomics* 2013;14:873.
53 Schwalm ND, Townsend GE, Groisman EA. Multiple Signals Govern Utilization of a Polysaccharide in the Gut Bacterium *Bacteroides thetaiotaomicron*. *MBio* 2016;7:e01342-16.
54 Wexler HM. Bacteroides: the good, the bad, and the nitty-gritty. *Clin Microbiol Rev* 2007;20:593–621.
55 Ravussin Y, Koren O, Spor A, *et al*. Responses of gut microbiota to diet composition and weight loss in lean and obese mice. *Obesity* 2012;20:738–47.
56 Schneeberger M, Everard A, Gómez-Valadés AG, *et al*. *Akkermansia muciniphila* inversely correlates with the onset of inflammation, altered adipose tissue metabolism and metabolic disorders during obesity in mice. *Sci Rep* 2015;5:16643.
57 Qiao Y, Sun J, Xia S, *et al*. Effects of different *Lactobacillus reuteri* on inflammatory and fat storage in high-fat diet-induced obesity mice model. *J Funct Foods* 2015;14:424–34.

58 Xin J, Zeng D, Wang H, *et al*. Preventing non-alcoholic fatty liver disease through *Lactobacillus johnsonii* BS15 by attenuating inflammation and mitochondrial injury and improving gut environment in obese mice. *Appl Microbiol Biotechnol* 2014;98:6817–29.

59 Pedersen HK, Gudmundsdottir V, Nielsen HB, *et al*. Human gut microbes impact host serum metabolome and insulin sensitivity. *Nature* 2016;535:376–81.

SUPPLEMENTARY MATERIAL

Supplementary methods

Energy intake and feces lipid content

The amount of food consumed was monitored from each cage and converted to daily intake per mouse. Average daily energy intake was calculated by converting the amount of food consumed into joules using the information provided by the diet manufacturer (LabDiet, TestDiet, USA). Lipid extraction for feces lipid content analysis was performed based on established procedures.[1]

Cecal and colonic short-chain fatty acids

Short-chain fatty acids (SCFAs), including acetate, propionate and butyrate, were measured in cecal and colonic samples using gas chromatography (6890N, Agilent Technologies, USA).[2] Supernatants (2 ml) were prepared by reconstituting all cecal content of each animal in 0.01 M of PBS, followed by centrifugation at 9,000g for 5 min at 4°C. Supernatants were acidified with nine volumes of 50% H_2SO_4 and extracted with ethyl ether. SCFA concentrations were measured in the organic phase using a gas chromatograph equipped with a polar HP-FFAP capillary column (0.25 mm × 0.25 mm × 30 m) and a flame ionization detector (Agilent Technologies). Helium was used as the carrier gas. Oven temperature was set at 140°C. Temperature was maintained for 10 min, raised to 165°C at 5°C/min, increased to 270°C at 25°C/min, and held at this temperature for 2 min. Detector temperature was set at 280°C and the injector temperature was 250°C. SCFAs were quantified by comparing peak areas with those of chemical standards. Data were obtained with the Agilent ChemStation (version G2070AA, Agilent Technologies).

Histopathological staining and scoring

Visceral adipose tissues (VATs), brown adipose tissues (BATs) and inguinal white adipose tissues (iWATs) were dissected and weighed following animal sacrifice. Subsections were partially embedded in 10% neutral buffered formalin (NBF) solution (Sigma, USA). The hepatic central lobe was collected and punched sections were fixed in 10% NBF. Paraffin-embedded hepatic central lobe and adipose tissue sections (4 μm) were stained with hematoxylin and eosin (H&E) for morphological examination. Slides were scanned with the NanoZoomer 2.0-HT slide scanner (Hamamatsu, Germany) and scanned sections were captured using Aperio

ImageScope (Leica Biosystems Imaging, USA). Quantification of adipocyte size was performed from five microscopy fields for each mouse using the Adiposoft software (Image J). The number of crown-like structures (CLS) consisting of dead adipocytes surrounded by macrophages was quantified. Scoring of non-alcoholic steatohepatitis activity index (NAI) was done based on five parameters described in a previous study,[3] including microvesicular steatosis, macrovesicular steatosis, hepatocellular hypertrophy, inflammation and fibrosis (supplementary dataset S1).

Immunohistochemistry staining

Immunohistochemistry staining (IHC) was performed on 4 μm paraffin-embedded sections using the Benchmark XT slide staining system combined with the OptiView DAB IHC Detection Kit (Ventana Medical Systems, USA) according to the manufacturer's protocol. Sections were hybridized with rabbit-anti-mouse uncoupling protein 1 antibody (UCP1, dilution 1:70, Proteintech, USA), exposed to 3,3-diaminobenzidine (DAB). Cell nuclei were counterstained with hematoxylin. Slides were scanned and observed as above.

Serum biochemical analysis

Biochemical analysis of serum samples was performed using an automatic Hitachi 7080 Chemistry Analyzer (Hitachi, Japan) based on the information provided by the manufacturer.

Oral glucose tolerance test and insulin tolerance test

For the oral glucose tolerance test (OGTT), 8-hr-fasted mice were treated with a glucose solution (10%, w/v) by intragastric gavage (1 g/kg). For the insulin tolerance test (ITT), 6-hr-fasted mice were injected intraperitoneally with insulin (0.5 IU/kg). Blood glucose levels were measured from tail vein blood using a glucometer (OneTouch Glucose Meters, USA). Total area under the curve (AUC) was calculated using the trapezoidal method.[4]

RNA extraction and quantitative real-time PCR analysis

Total RNA was extracted from proximal colon tissues using the Tri Reagent Kit (Sigma, USA) according to the manufacturer's instructions. Equal amounts of RNA were used to synthesize cDNA using the Quant II fast RT kit (Tools, Taiwan). cDNA was used for quantitative real-time PCR (qRT-PCR) with the KAPA SYBR FAST

Universal 2× qPCR Master Mix (Kapa Biosystems, USA). Expression of IL-1β, TNF-α, ZO-1 and the housekeeping gene glyceraldehyde-3-phosphate dehydrogenase (GAPDH) was assessed by qRT-PCR. Relative amount of transcripts for target genes was determined for each cDNA sample after normalization against GAPDH or 18S rRNA. Data were analyzed using the $2^{-\Delta\Delta CT}$ method.[5] Primer sequences for qRT-PCR are shown in supplementary table S4.

Flow cytometry analysis

Isolation of mononuclear cells in mouse colonic lamina propria was performed as described previously.[6] Flow cytometry analysis was performed using a FACSCalibur flow cytometer (BD, USA). Data were analyzed using the FlowJo software (v.9.3.2, FlowJo, USA). IL-1β-expressing M1 macrophages were first gated with the F4/80 positive population and identified as CD11c and IL-1β double-positive cells. IL-10-expressing regulatory T cells were first gated with the CD4 positive population and identified as Foxp3 and IL-10 double-positive cells.

Fecal microbiota transplantation

Chow- and HFD-fed donor mice (5-week old, male) were treated daily with saline, HSM, H1 and H4 via oral gavage for 4 weeks, followed by daily collection of feces. Feces pellets (80–110 mg) from each donor mice were collected daily in autoclaved tubes and homogenized in 1 ml of sterile saline. Homogenized fecal mixtures were centrifuged for 1 min at 2,000g at 4°C. Supernatants were transferred to new tubes and centrifuged for 5 min at 15,000g to precipitate bacteria. Bacterial pellets were resuspended in 600 μl of sterile saline. HFD-fed mice (5-week old, male) were inoculated daily with 100 μl of fecal microbiota transplants from each donor group via oral gavage for 12 weeks (supplementary figures 10–12). The FMT procedure from collection of fecal microbiota to oral gavage was completed within 1 hr.

Cecal microbiota DNA extraction

Cecal microbiota DNA was extracted using the QIAamp DNA Stool Mini Kit (Qiagen, USA). Cecal content (in vivo antibiotics treatment and recipients of ex FMT) and fecal pellets (donors of ex FMT) were added to a tube containing a sterilized steel bead, prior to treatment as described in the manufacturer's instructions. Tubes containing specimen and steel bead were placed into a benchtop homogenizer (TissueLyser II, Qiagen) and disrupted for 30 seconds three times, with a 1-min rest

period. Microbiota samples were collected by low-speed centrifugation and high-speed centrifugation after homogenization, and further treated as described in the manufacturer's instructions. DNA concentration was measured using the NanoPhotometer P360 (Implen, USA).

Illumina HiSeq sequencing and library construction

Cecal or fecal samples were snap-frozen in liquid nitrogen and stored at –80°C. DNA was extracted using a fecal DNA isolation kit (Qiagen). 16S rRNA gene comprising the V3–V4 regions was amplified using composite primers containing a unique 10-base barcode to tag PCR products. PCR mix (50 µl) contained 25 ng DNA template, 5× HiFi buffer, 10 mM dNTP mix, 1 unit/µl HiFi DNA polymerase (KAPA Biosystems, USA) and 0.3 µM of composite primer pairs. PCR reaction conditions consisted of denaturation at 95°C for 3 min, followed by 15–25 cycles of 98°C for 20 sec, 45°C for 15 sec, and 72°C for 15 sec, and a final extension of 72°C for 1 min. Composite primers consisted of the forward primer 5'-TCGTCGGCAGCGTCAGATGTGTATAAGAGACAG*CCTAYGGGRBGCASCAG*-3', which contains the Illumina forward overhang adaptor sequence (underlined) and the universal bacterial primer 341F (italicized), and the reverse primer 5'-GTCTCGTGGGCTCGGAGATGTGTATAAGAGACAG*GGACTACNNGGGTATCTAAT*-3', which contains the Illumina reverse overhang adaptor sequence (underlined) and the broad-range bacterial primer 806R (italicized). Replicate PCRs were pooled and amplicons were purified using the QiaQuick PCR Purification Kit (Qiagen). PCR amplicons were sequenced using the Illumina sequencing platform following the instructions of the manufacturer and HiSeq procedures. Sequencing libraries were generated using the TruSeq DNA PCR-Free Sample Preparation Kit (Illumina, USA) following the manufacturer's recommendations. Library quality was assessed using the Qubit@ 2.0 Fluorometer (Thermo Scientific) and Agilent Bioanalyzer 2100 system. The library was sequenced on an Illumina HiSeq 2500 platform and 250 bp paired-end reads were generated. Sequence datasets were deposited into the Sequence Read Archive (accession numbers SRP139890 and SRP139903).

16S rDNA-based metagenomics analysis

Amplicon sequencing was performed using 250 bp paired-end raw reads and the entire paired-end reads were assembled using FLASH v.1.2.7.[7] Low-quality reads (Q score <20) were discarded in QIIME 1.7.[8] If three consecutive bases were <Q20, the

read was truncated and the resulting read was retained in the data only if it was at least 75% of the original length[9] (QIIME script split_libraries_fastq.py). Sequences were chimera-checked using UCHIME[10, 11] and filtered from the data set before operational taxonomic unit (OTU) picking of 97% sequence identity using USEARCH v.7 pipeline[12] (UPARSE function).[13] For each representative sequence, the Greengenes Database version 13_8[14, 15] was used based on RDP classifier (v.2.2) algorithm[16] to annotate taxonomy classification. Any sequences presented once (singletons) or in only one sample were filtered out. In order to identify the relationship between different OTUs, multiple sequence alignment was conducted using the PyNAST software (v.1.2)[17] against the core-set dataset in the Greengenes database. A phylogenetic tree was constructed with a set of sequences representative of the OTUs using the FastTree,[18, 19] which was already included in QIIME. To avoid sampling depth bias, OTUs abundance information was rarefied to the minimum sequences across samples by random sampling (without replacement) of the raw OTU abundance (QIIME script single_rarefaction.py). Beta diversity analysis was used to evaluate differences of samples in species complexity. Beta diversity on weighted UniFrac[20, 21] was calculated using the QIIME software. Principal coordinate analysis (PCoA) was performed to obtain principal coordinates and visualize complex, multidimensional data. PCoA analysis was displayed using the WGCNA package, stat packages and ggplot2 package of the R software (v.2.15.3). To analyse significant differences between groups, permutational multivariate analysis of variance (PERMANOVA) tests (9,999 permutations) were performed on the weighed UniFrac distance matrices using QIIME. Unweighted pair-group method with arithmetic means (UPGMA) clustering was performed as a type of hierarchical clustering method to interpret the distance matrix using average linkage using the QIIME software. For comparing metagenomic samples, significance of all species between groups on various taxonomic levels were tested using Metastats.[22] The *P* values of comparison between two groups were calculated using an equation suggested in the Metastats software, when less than 8 subjects were used in each treatment. OTUs were searched against the GenBank sequence database (National Center for Biotechnology Information, NCBI, USA; assignment was based on >97% identity and 100% coverage of 16S rRNA genes). Heatmaps were drawn using MeV version 4.8.1.

Quantification of fecal and cecal microbiota by quantitative PCR

Levels of *P. goldsteinii* in fecal and cecal microbiota were determined using real-time

quantitative PCR (7900HT, Applied Biosystems, USA) and specific primers (supplementary table S4), along with the KAPA SYBR FAST master mix (2×) qPCR kit (Kapa Biosystems, USA). Standard curves were determined from the CT values of serial diluted plasmid (pHE vector, Biotools, Taiwan) containing single copy of full-length of *P. goldsteinii* which is amplified using 16S rDNA V1–V9 primers (supplementary table S4). The absolute copy number of targeted bacteria was calculated using a standard curve.

Supplementary references

1. Kraus D, Yang Q, Kahn BB. Lipid extraction from mouse feces. *Bio Protoc* 2015;5.
2. Wu PS, Kuo YT, Chen SM, Li Y, Lou BS. Gas chromatography-mass spectrometry analysis of photosensitive characteristics in citrus and herb essential oils. *J Chromatogr Sep Tech* 2014;6.
3. Liang W, Menke AL, Driessen A, *et al.* Establishment of a general NAFLD scoring system for rodent models and comparison to human liver pathology. *PLoS One* 2014;9:e115922.
4. Purves RD. Optimum numerical integration methods for estimation of area-under-the-curve (AUC) and area-under-the-moment-curve (AUMC). *J Pharmacokinet Biopharm* 1992;20:211–26.
5. Livak KJ, Schmittgen TD. Analysis of relative gene expression data using real-time quantitative PCR and the 2(T)(-Delta Delta C) method. *Methods* 2001;25:402–408.
6. Weigmann B, Tubbe I, Seidel D, *et al.* Isolation and subsequent analysis of murine lamina propria mononuclear cells from colonic tissue. *Nat Protoc* 2007;2:2307–11.
7. Magoc T, Salzberg SL. FLASH: fast length adjustment of short reads to improve genome assemblies. *Bioinformatics* 2011;27:2957–63.
8. Caporaso JG, Kuczynski J, Stombaugh J, *et al.* QIIME allows analysis of high-throughput community sequencing data. *Nat Methods* 2010;7:335–6.
9. Bokulich NA, Subramanian S, Faith JJ, *et al.* Quality-filtering vastly improves diversity estimates from Illumina amplicon sequencing. *Nat Methods* 2013;10:57–U11.
10. Edgar RC, Haas BJ, Clemente JC, *et al.* UCHIME improves sensitivity and speed of chimera detection. *Bioinformatics* 2011;27:2194–2200.
11. Haas BJ, Gevers D, Earl AM, *et al.* Chimeric 16S rRNA sequence formation and detection in Sanger and 454-pyrosequenced PCR amplicons. *Genome Res* 2011;21:494–504.
12. Edgar RC. Search and clustering orders of magnitude faster than BLAST. *Bioinformatics* 2010;26:2460–2461.
13. Edgar RC. UPARSE: highly accurate OTU sequences from microbial amplicon reads. *Nat Methods* 2013;10:996–8.
14. DeSantis TZ, Hugenholtz P, Larsen N, *et al.* Greengenes, a chimera-checked 16S

rRNA gene database and workbench compatible with ARB. *Appl Environ Microbiol* 2006;72:5069–72.

15. McDonald D, Price MN, Goodrich J, *et al.* An improved Greengenes taxonomy with explicit ranks for ecological and evolutionary analyses of bacteria and archaea. *ISME J* 2012;6:610–8.
16. Wang Q, Garrity GM, Tiedje JM, *et al.* Naive Bayesian classifier for rapid assignment of rRNA sequences into the new bacterial taxonomy. *Appl Environ Microbiol* 2007;73:5261–7.
17. Caporaso JG, Bittinger K, Bushman FD, *et al.* PyNAST: a flexible tool for aligning sequences to a template alignment. *Bioinformatics* 2010;26:266–267.
18. Price MN, Dehal PS, Arkin AP. FastTree: computing large minimum evolution trees with profiles instead of a distance matrix. *Mol Biol Evol* 2009;26:1641–50.
19. Price MN, Dehal PS, Arkin AP. FastTree 2—approximately maximum-likelihood trees for large alignments. *PLoS One* 2010;5:e9490.
20. Lozupone C, Knight R. UniFrac: a new phylogenetic method for comparing microbial communities. *Appl Environ Microbiol* 2005;71:8228–35.
21. Lozupone C, Lladser ME, Knights D, *et al.* UniFrac: an effective distance metric for microbial community comparison. *ISME J* 2011;5:169–72.
22. White JR, Nagarajan N, Pop M. Statistical methods for detecting differentially abundant features in clinical metagenomic samples. *PLoS Computational Biol* 2009;5.
23. Chang CJ, Lin CS, Lu CC, *et al.* Ganoderma lucidum reduces obesity in mice by modulating the composition of the gut microbiota. *Nat Commun* 2015;6:7489.
24. Tang K, Pasqua T, Biswas A, *et al.* Muscle injury, impaired muscle function and insulin resistance in Chromogranin A-knockout mice. *J Endocrinol* 2017;232:137–153.
25. Ehara T, Kamei Y, Takahashi M, *et al.* Role of DNA methylation in the regulation of lipogenic glycerol-3-phosphate acyltransferase 1 gene expression in the mouse neonatal liver. *Diabetes* 2012;61:2442–50.
26. Miyata S, Inoue J, Shimizu M, *et al.* Xanthohumol improves diet-induced obesity and fatty liver by suppressing sterol regulatory element-binding protein (SREBP) Activation. *J Biol Chem* 2015;290:20565–79.
27. Shostak A, Meyer-Kovac J, Oster H. Circadian regulation of lipid mobilization in white adipose tissues. *Diabetes* 2013;62:2195–203.
28. Reid BN, Ables GP, Otlivanchik OA, *et al.* Hepatic overexpression of

hormone-sensitive lipase and adipose triglyceride lipase promotes fatty acid oxidation, stimulates direct release of free fatty acids, and ameliorates steatosis. *J Biol Chem* 2008;283:13087–99.

29. Penna F, Busquets S, Toledo M, *et al.* Erythropoietin administration partially prevents adipose tissue loss in experimental cancer cachexia models. *J Lipid Res* 2013;54:3045–51.
30. Estall JL, Kahn M, Cooper MP, *et al.* Sensitivity of lipid metabolism and insulin signaling to genetic alterations in hepatic peroxisome proliferator-activated receptor-gamma coactivator-1alpha expression. *Diabetes* 2009;58:1499–508.
31. Bu SY, Mashek MT, Mashek DG. Suppression of long chain acyl-CoA synthetase 3 decreases hepatic de novo fatty acid synthesis through decreased transcriptional activity. *J Biol Chem* 2009;284:30474–83.
32. Li G, Xie C, Lu S, *et al.* Intermittent fasting promotes white adipose browning and decreases obesity by shaping the gut microbiota. *Cell Metab* 2017;26:672–685.
33. Babkair H, Yamazaki M, Uddin MS, *et al.* Aberrant expression of the tight junction molecules claudin-1 and zonula occludens-1 mediates cell growth and invasion in oral squamous cell carcinoma. *Hum Pathol* 2016;57:51–60.
34. Muralidharan S, Ambade A, Fulham MA, *et al.* Moderate alcohol induces stress proteins HSF1 and hsp70 and inhibits proinflammatory cytokines resulting in endotoxin tolerance. *J Immunol* 2014;193:1975–87.
35. Obata T, Goto Y, Kunisawa J, *et al.* Indigenous opportunistic bacteria inhabit mammalian gut-associated lymphoid tissues and share a mucosal antibody-mediated symbiosis. *Proc Natl Acad Sci U S A* 2010;107:7419–24.

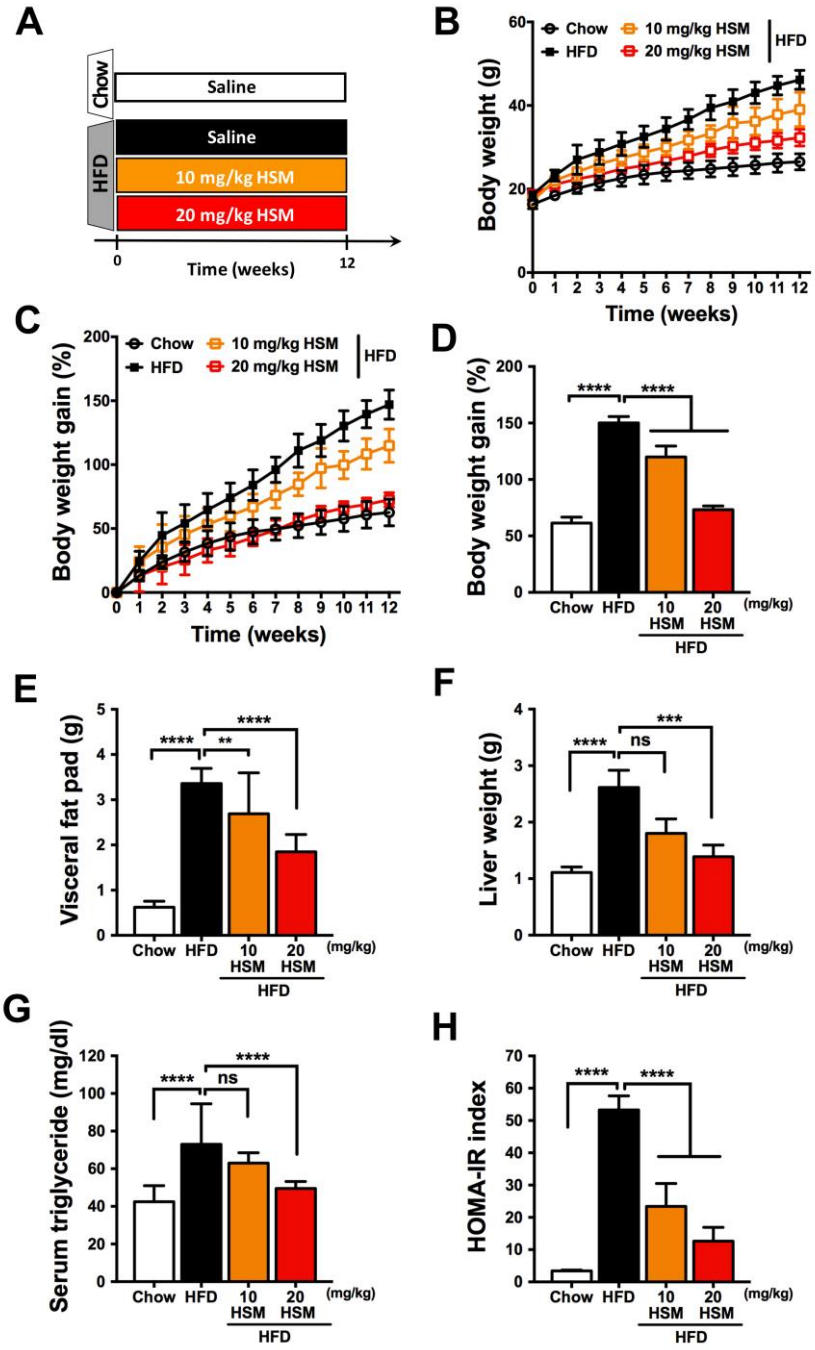

Supplementary figure S1

HSM reduces obesity in HFD-fed mice. (A) Chow-fed mice and HFD-fed mice were treated with control saline or HSM (10 or 20 mg/kg) by oral gavage for 12 weeks. (B) Body weight and (C) body weight gain were monitored throughout the 12-week period. Obesity traits including (D) body weight gain, (E) visceral fat pad weight (epididymal white adipose tissue), (F) liver weight, (G) serum triglycerides and (H) HOMA-IR index were assessed after 12 weeks of treatments. Data are presented as means ± SD. n=14 to 15 for panels B–E; n=9 to 10 for panels F,G. Data were analyzed using one-way ANOVA followed by Bonferroni's post hoc test. **p<0.01; ***p<0.001; ns, not significant.

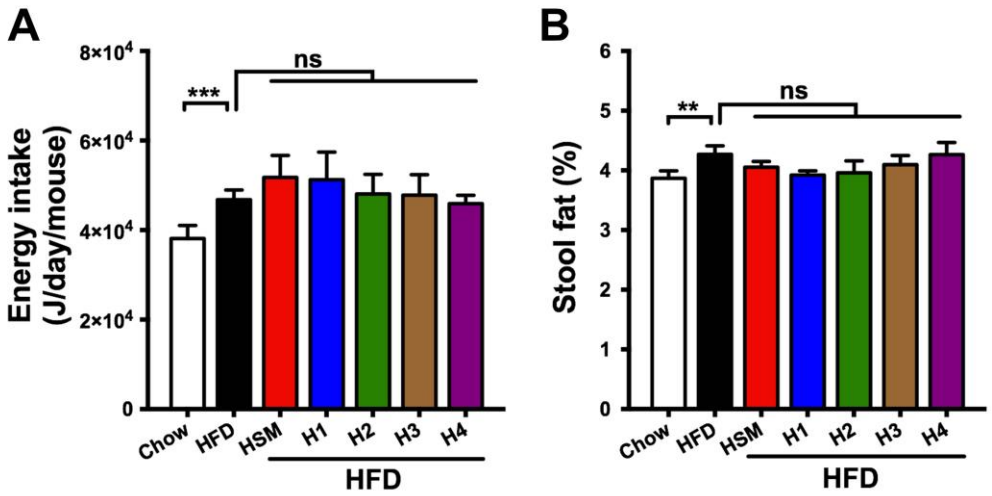

Supplementary figure S2

HSM and polysaccharide fractions do not affect energy intake or lipid absorption in HFD-fed mice. Experiments were performed as in figure 1. Fractions H1–H4 were given at 20 mg/kg by oral gavage for 12 weeks. (A) Average daily energy intake (n=10 mice/group). (B) Fecal lipid content. Data are shown as means ± SD (n=5 mice/group). Data were analyzed using one-way ANOVA followed by Bonferroni's post hoc test. **p<0.01; ***p<0.001; ns, not significant.

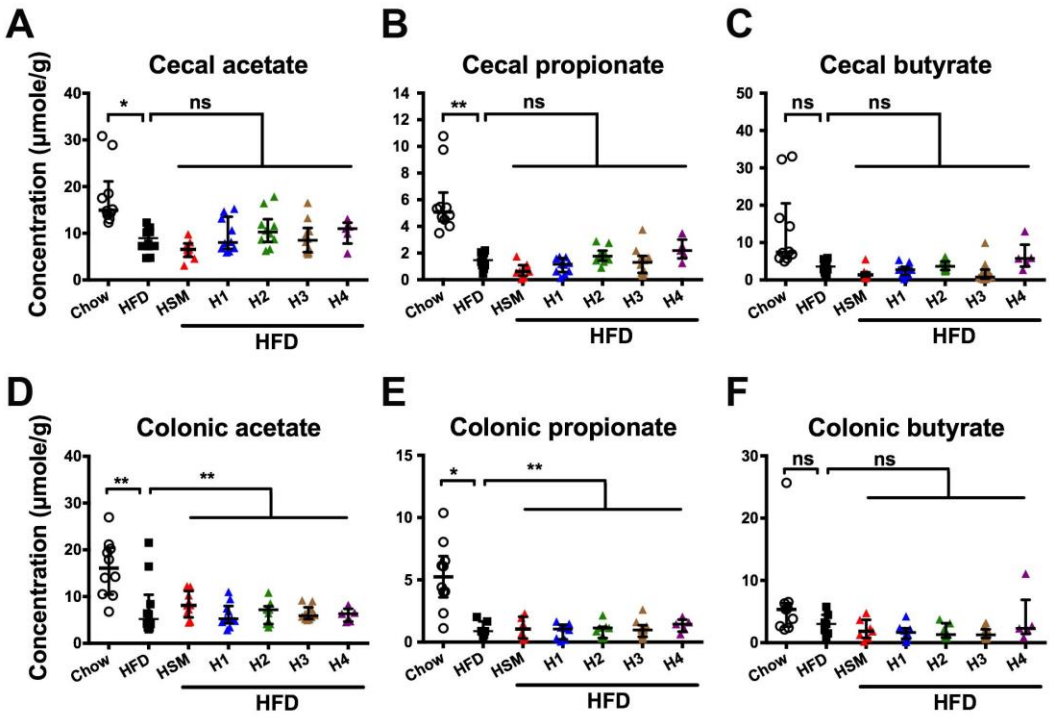

Supplementary figure S3

HSM and polysaccharide fractions do not affect intestinal production of short chain fatty acids. Experiments were performed as in figure 1. Acetate, propionate and butyrate were quantified in (A–C) cecum or (D–F) colon of chow-fed and HFD-fed mice after 12 weeks of treatment. Data represent medians ± interquartile range (IQR) (n=5 to 10 mice/group). Data were analyzed using Kruskal-Wallis test with Dunn's post hoc test. *p<0.05; **p<0.01; ns, not significant.

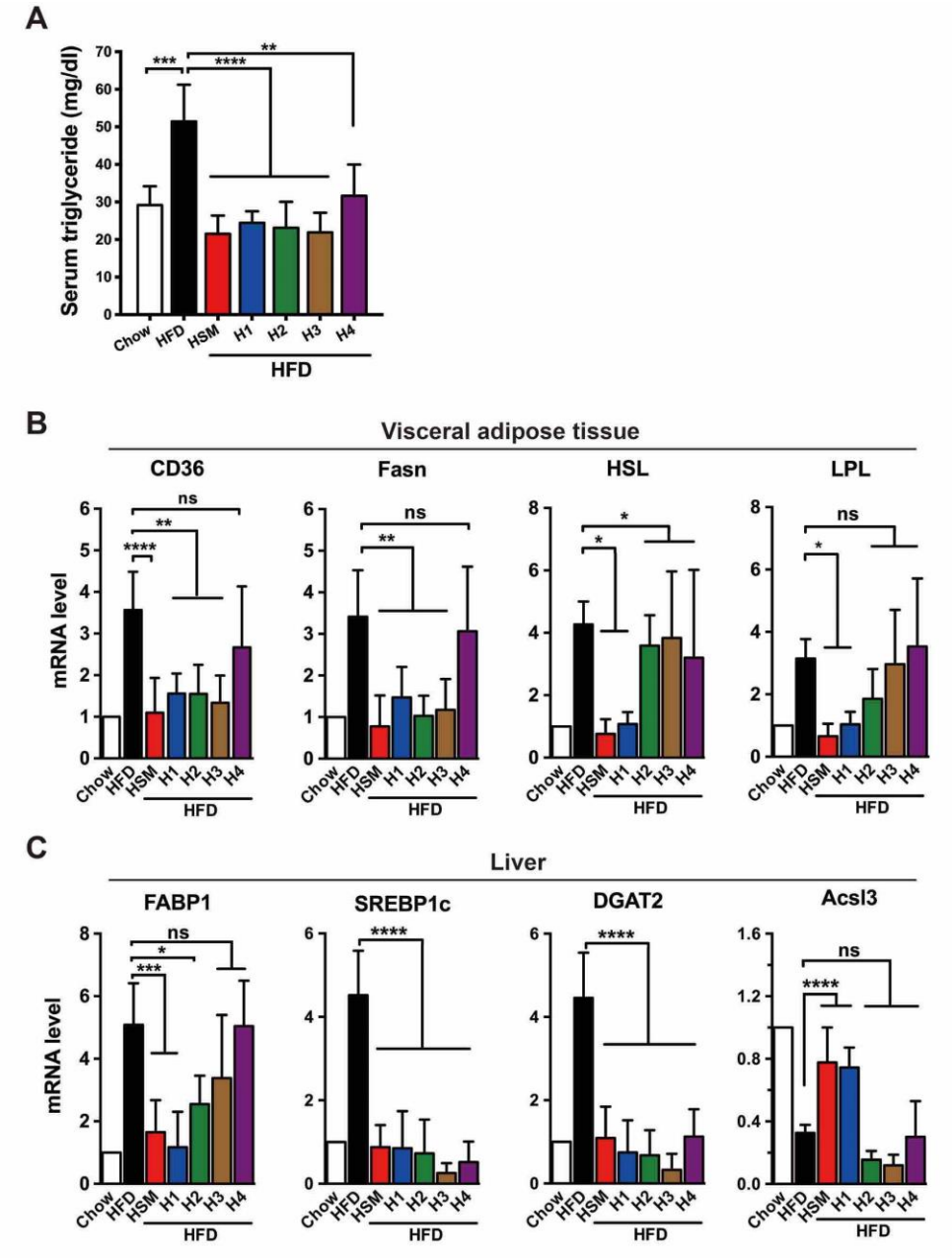

Supplementary figure S4

Effects of HSM and polysaccharide fractions on serum triglycerides and gene expression involved in lipid metabolism. Experiments were performed as in figure 1. (A) Serum triglycerides (n=5 per group). qRT-PCR analysis of lipid metabolism genes in (B) visceral adipose and (C) hepatic tissues. The genes examined are involved in lipid transport and uptake (cluster of differentiation 36, CD36; fatty acid-binding protein 1, FABP1), lipogenesis (diglyceride acyltransferase, DGAT2; fatty acid synthase, Fasn; sterol regulatory-element binding protein 1c, SREBP1c), lipolysis (hormone-sensitive lipase, HSL; lipoprotein lipase, LPL) or β-oxidation (long-chain-fatty-acid-CoA ligase 3, Acsl3). Data represent means ± SD (n=5 to 10 mice/group). Data were analyzed using one-way ANOVA followed by Bonferroni's post hoc test. *p<0.05; **p<0.01; ***p<0.001; ****p<0.0001; ns, not significant.

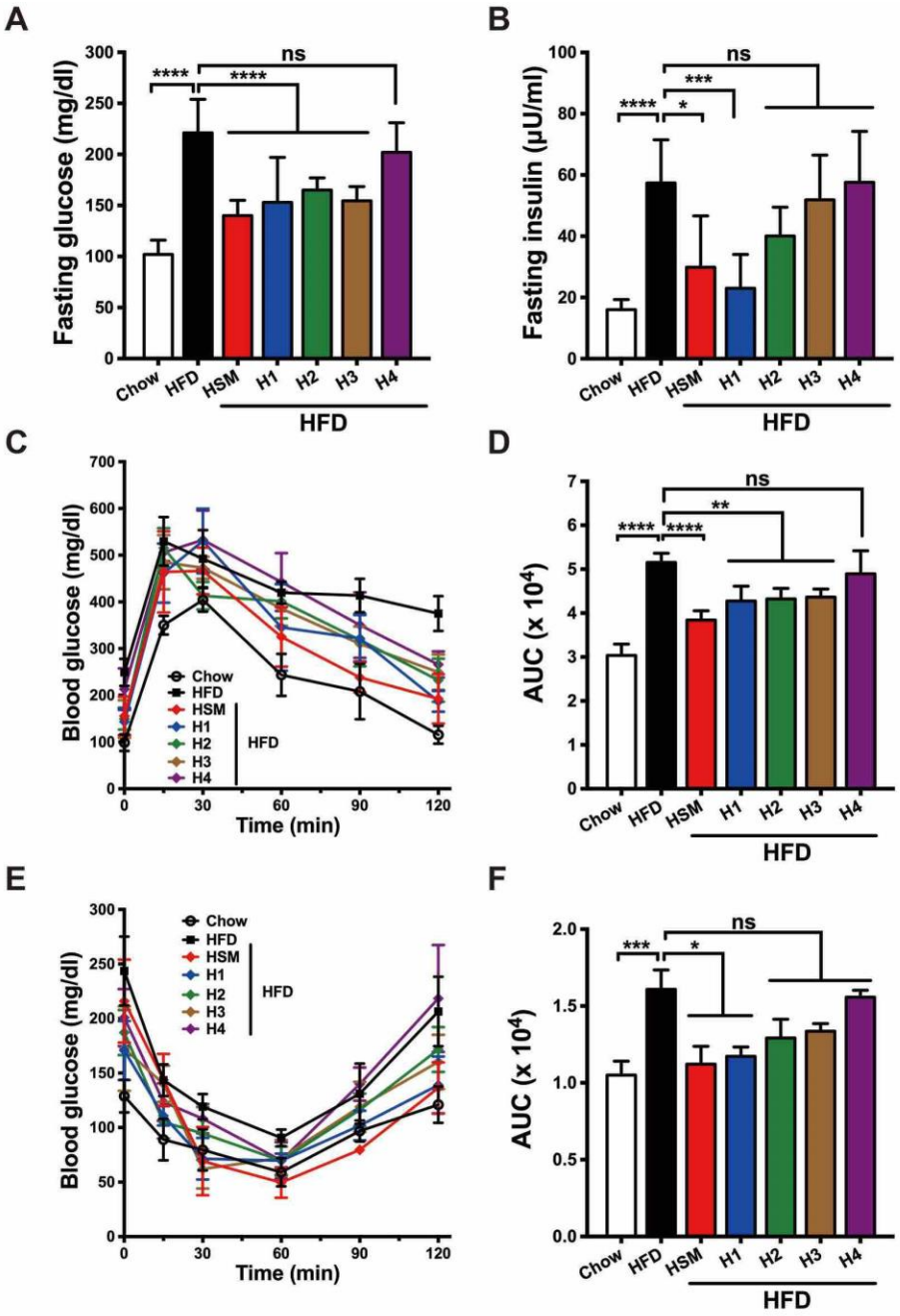

Supplementary figure S5

HSM and H1 restore glucose and insulin sensitivity in HFD-induced obese mice. Experiments were performed as in figure 1. (A) Fasting blood glucose and (B) fasting serum insulin. (C) OGTT and (D) the corresponding area under the curve (AUC). (E) ITT and (F) the corresponding AUC values. Data represent means ± SD (n=10 to 15 mice for panels A,B; n=5 for panels C–F) and analyzed using one-way ANOVA followed by Bonferroni's post hoc test. *p<0.05; **p<0.01; ***p<0.001; ****p<0.0001; ns, not significant.

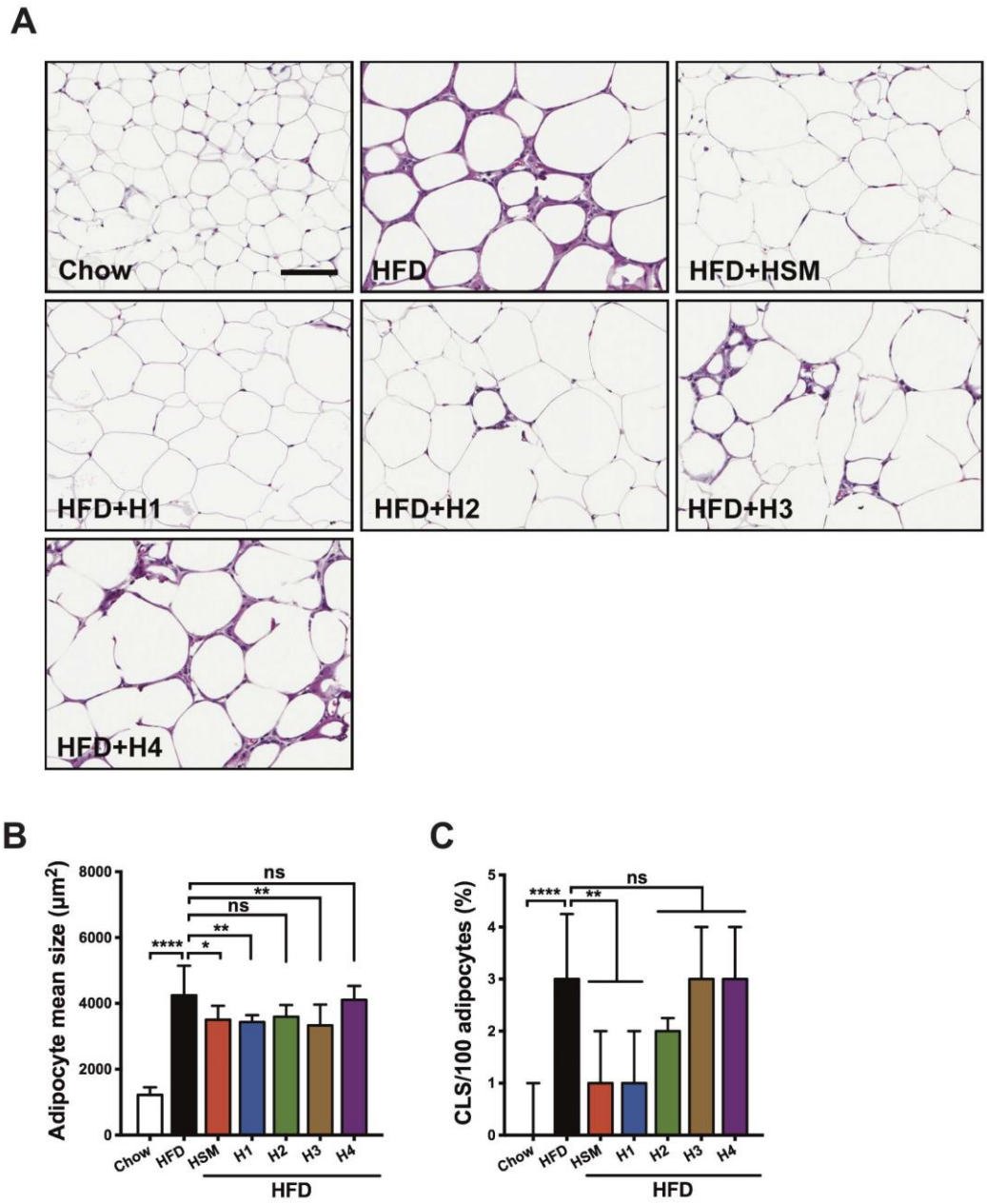

Supplementary figure S6

HSM and H1 reduce adipocyte hypertrophy and crown-like structures in HFD-fed mice. Experiments were performed as in figure 1. (A) Representative images of hematoxylin and eosin (H&E)-stained visceral adipose tissues. Scale bar, 100 µm. (B) Adipocyte size in visceral adipose tissues was determined from five microscopy fields for each mouse using Adiposoft (Image J). Data represent medians ± IQR (n=10 mice/group). Data were analyzed using the Kruskal-Wallis test with Dunn's post hoc test. (C) Quantification of crown-like structures (CLS; n=5 images per mouse) in visceral adipose tissues. Data represent means ± SD (n=10 mice/group). Data were analyzed using one-way ANOVA followed by Bonferroni's post hoc test. *p<0.05; **p<0.01; ***p<0.001; ****p<0.0001; ns, not significant.

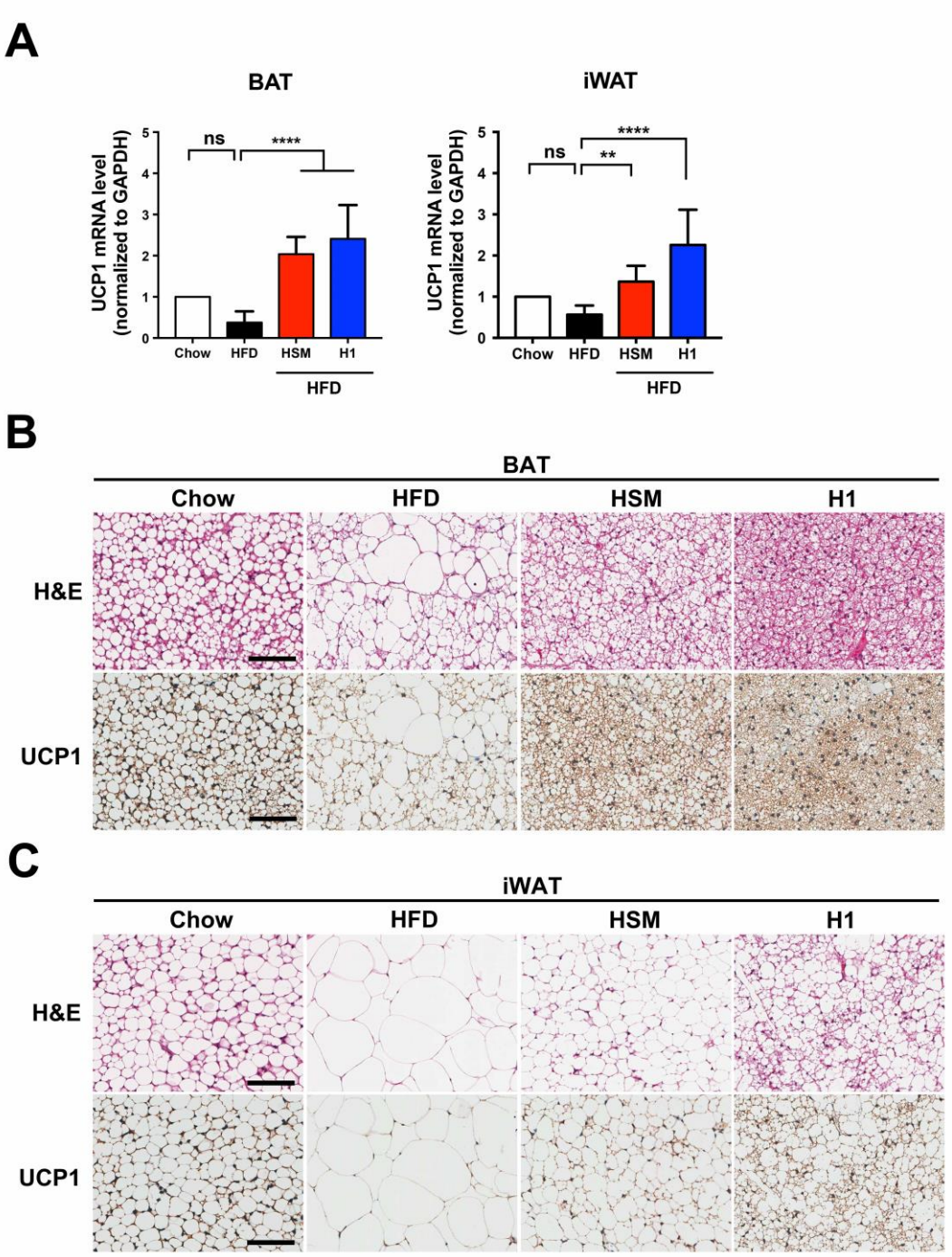

Supplementary figure S7

HSM and H1 induce expression of thermogenic protein markers in HFD-fed mice. (A) Quantitative real-time-PCR (qRT-PCR) analysis of mitochondrial uncoupling protein 1 (UCP1) gene expression in brown adipose tissues (BATs, left panel) and inguinal white adipose tissues (iWATs, right panel). Representative images of H&E-stained and UCP1-stained (B) BATs and (C) iWATs. Tissue slides that were cut in succession were used. Scale bars, 100 µm. Data represent means ± SD (n=5 mice/group). Data were analyzed using one-way ANOVA followed by Bonferroni's post hoc test. **p<0.01; ****p<0.0001; ns, not significant.

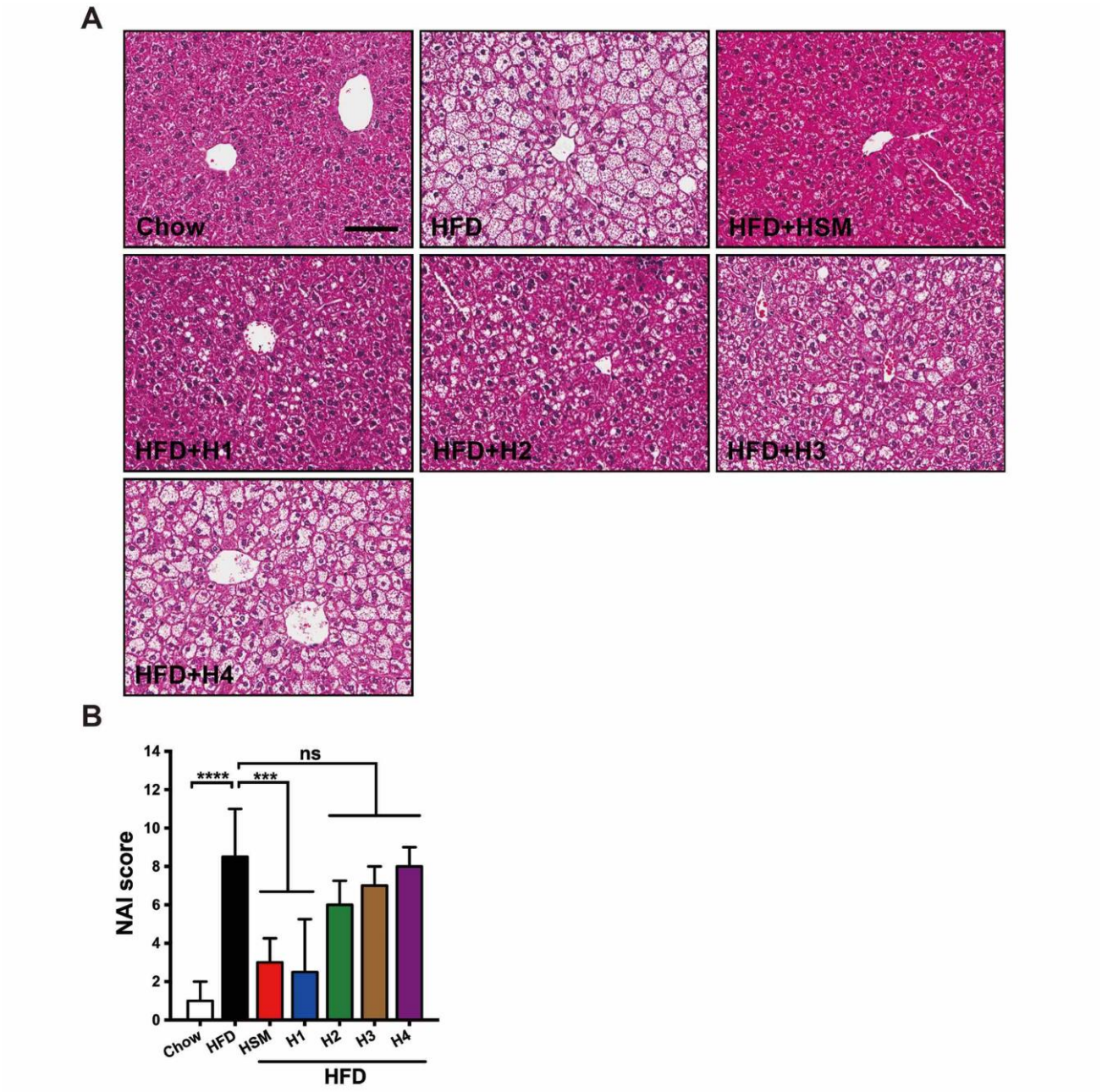

Supplementary figure S8

HSM and H1 reduce pathological signs of NAFLD and NASH in HFD-fed mice. Experiments were performed as in figure 1. (A) Representative images of H&E-stained liver tissues. Scale bar, 100 µm. (B) Non-alcoholic steatohepatitis (NASH) activity index (NAI; n=5 images per mouse). Data represent means ± SD (n=10 mice per group) and analyzed using one-way ANOVA followed by Bonferroni's post hoc test. ***p<0.001; ****p<0.0001; ns, not significant.

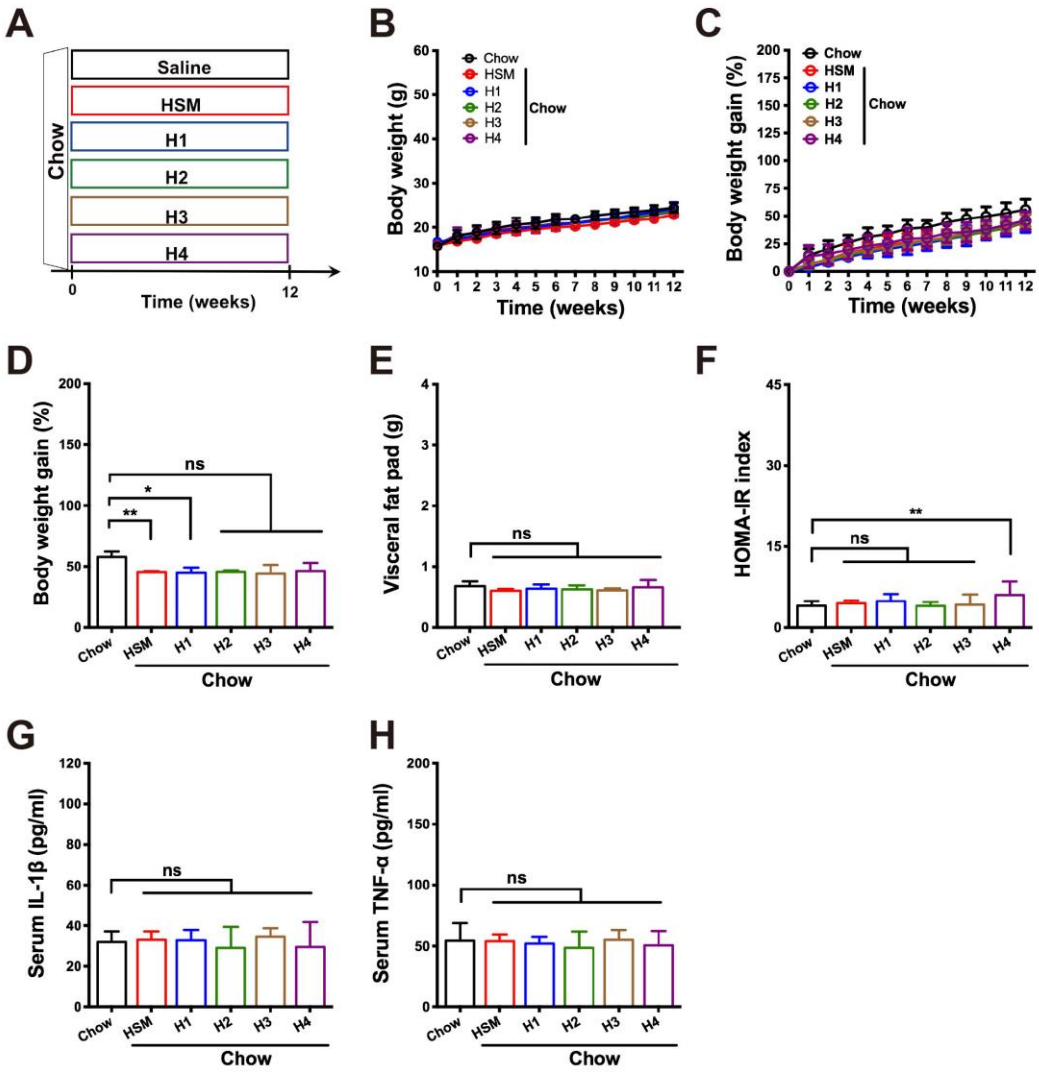

Supplementary figure S9

Effects of HSM and H1 treatment in chow-fed mice. (A) Chow-fed mice were treated daily with saline, HSM or fractions H1–H4 for 12 weeks as indicated. (B) Body weight was monitored for 12 weeks. Obesity traits including (C) body weight gain, (D) visceral fat pad weight, (E) HOMA-IR index, (F) serum IL-1β, and (G) serum TNF-α were measured after 12 weeks of treatments as described in Methods. Data are presented as means ± SD. n=10 to 15 mice/group for panels A–C,E; n=5 to 10 mice/group for panels D,F,G. Statistical analysis was performed using one-way ANOVA followed by Bonferroni's post hoc test. *p<0.05; **p<0.01; ns, not significant.

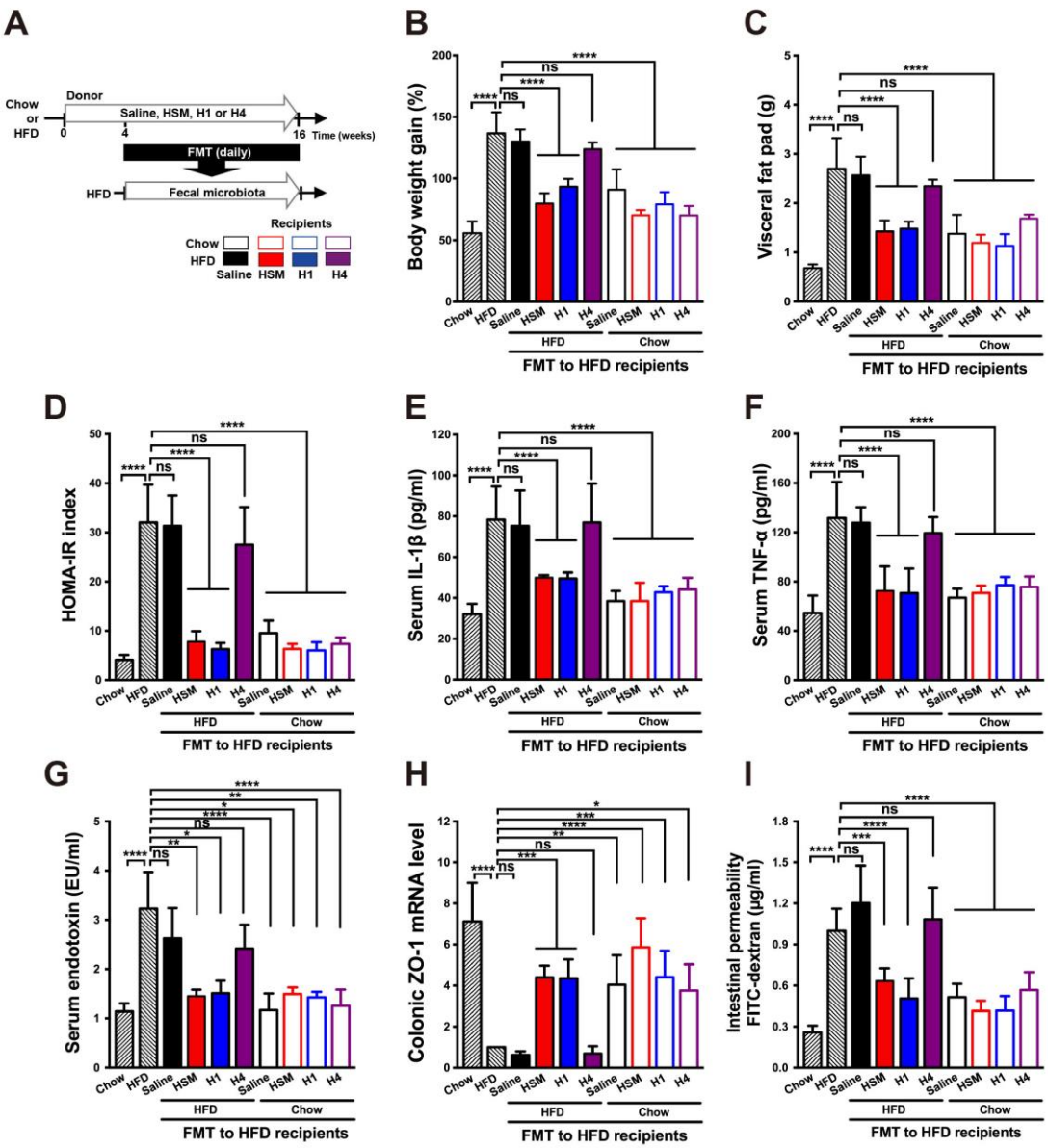

Supplementary figure S10

FMT from HSM- and H1-treated mice reduces obesity and metabolic disorders in HFD-fed recipient mice. (A) Diagram illustrating the horizontal FMT experiments performed. HFD-fed mice were treated with fecal microbiota from chow-fed donors or HFD-fed donors treated with saline, HSM, H1 or H4. Obesity traits consisting of (B) body weight gain, (C) visceral fat pad weight, (D) HOMA-IR index, (E) serum IL-1β, (F) serum TNF-α, (G) serum endotoxin, (H) colonic ZO-1 mRNA expression and (I) intestinal permeability were measured after 12 weeks of FMT. Data are presented as means ± SD and analyzed using one-way ANOVA followed by Bonferroni's post hoc test and false-discovery rate (FDR) correction for multiple testing. n=10 to 15 mice/group for panels B–G; n=5 to 15 mice/group for panels H–I. *p<0.05; **p<0.01; ***p<0.001; ****p<0.0001; ns, not significant.

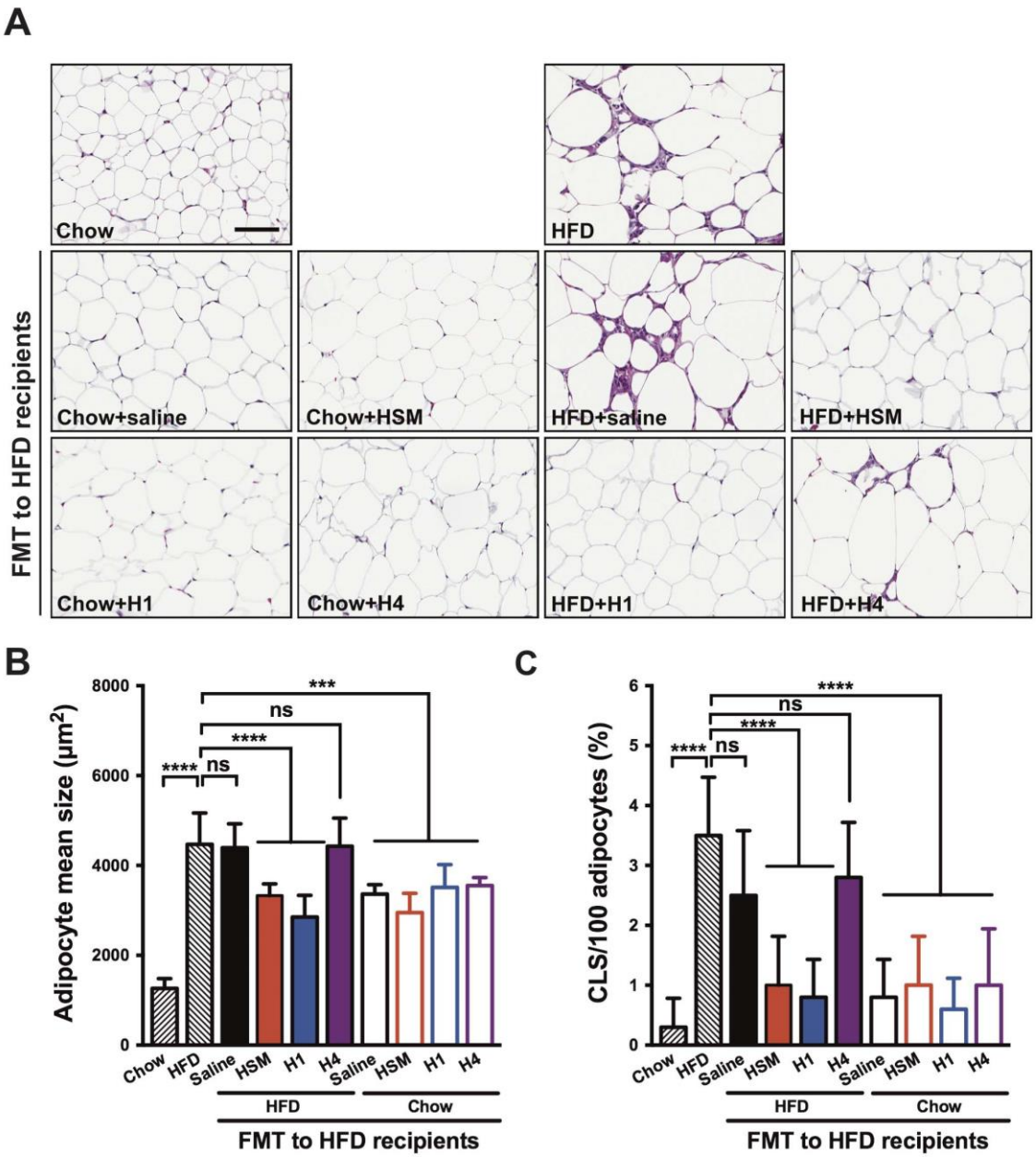

Supplementary figure S11

FMT from HSM- and H1-treated mice reduces adipocyte hypertrophy and crown-like structures in HFD-fed mice. Experiments were performed as in supplementary figure 10. (A) Representative images of H&E-stained visceral adipose tissues. Scale bar, 100 µm. (B) Mean adipocyte size in visceral adipose tissues was determined from five microscopy fields for each mouse using Adiposoft (Image J). Data represent medians ± IQR (n=10 mice/group). Data were analyzed using the Kruskal-Wallis test with Dunn's post hoc test. (C) Quantification of crown-like structures (CLS; n=5 images per mouse) in visceral adipose tissues. Data represent means ± SD (n=10 mice/group). Data were analyzed using one-way ANOVA followed by Bonferroni's post hoc test. ***p<0.001; ****p<0.0001; ns, not significant.

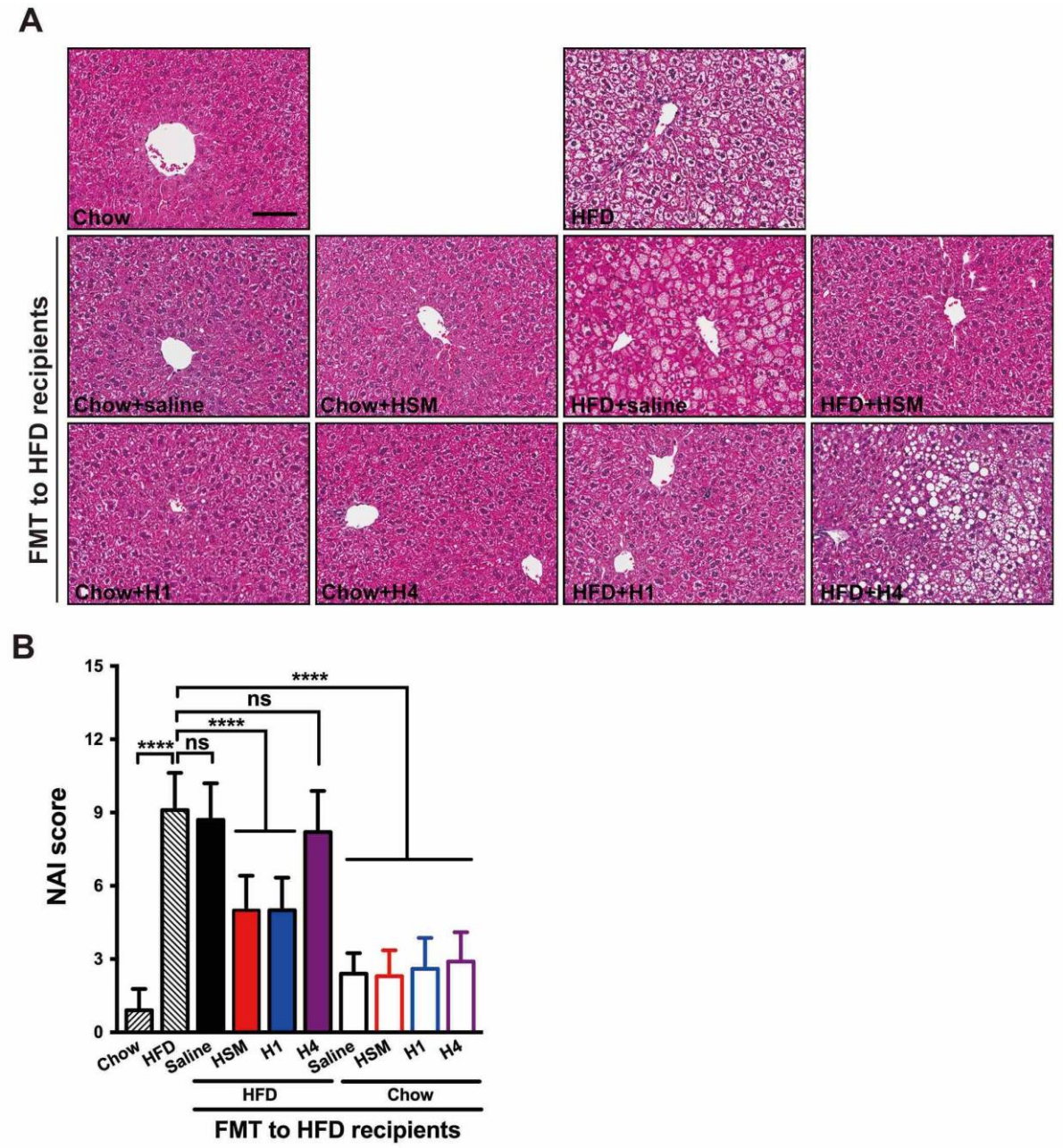

Supplementary figure S12

FMT from HSM- and H1-treated mice reduces NAFLD and NASH pathological changes. Experiments were performed as in supplementary figure 10. (A) Representative images of H&E-stained liver tissues. Scale bar, 100 µm. (B) NASH activity index (NAI; n=5 images per mouse). Data represent means ± SD (n=10 mice/group) analyzed using one-way ANOVA followed by Bonferroni's post hoc test. ****p<0.0001; ns, not significant.

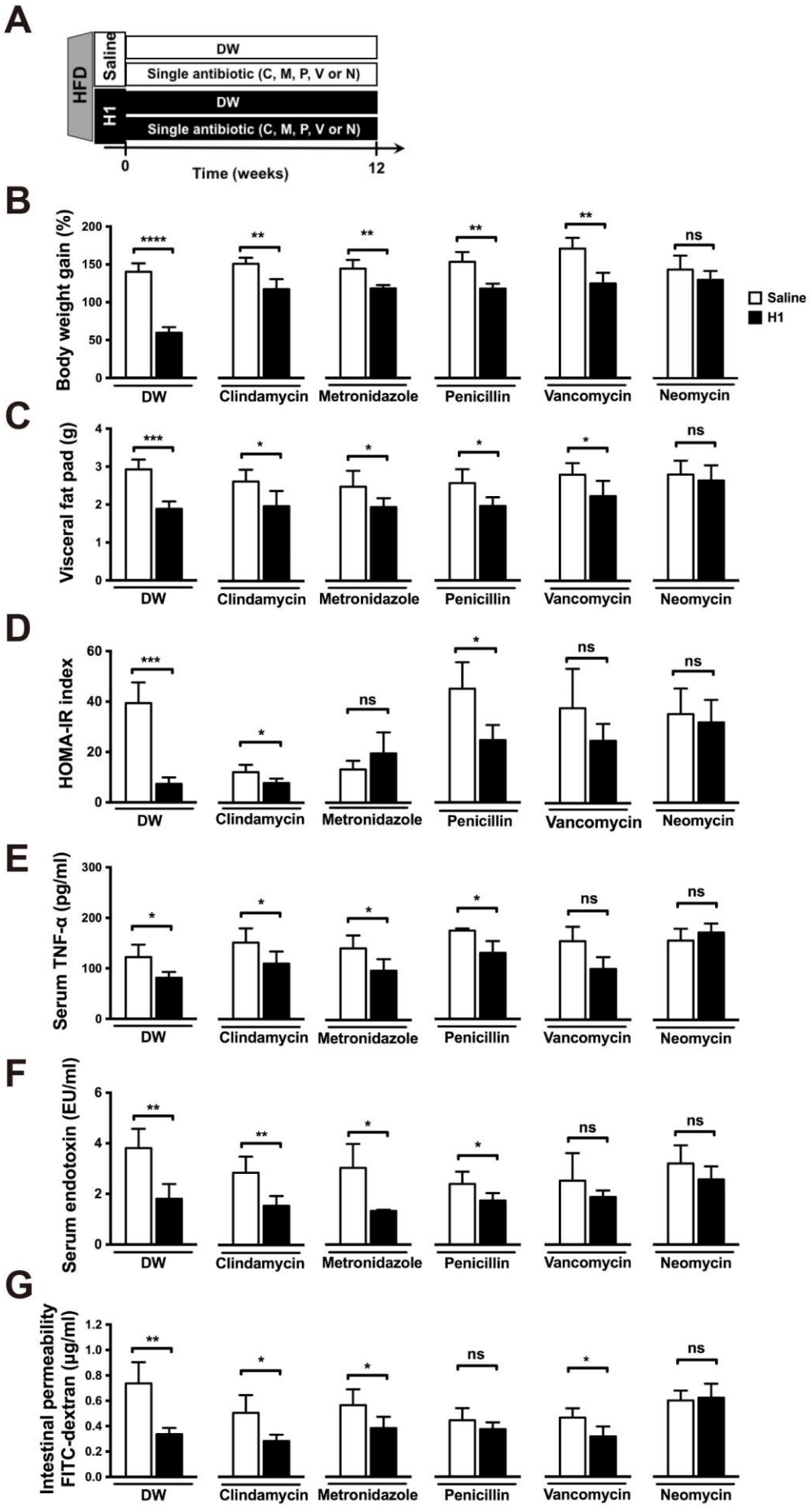
A
HFD
Saline
H1
DW
Single antibiotic (C, M, P, V or N)
DW
Single antibiotic (C, M, P, V or N)
0
Time (weeks)
12
B
Body weight gain (%)
C
Visceral fat pad (g)
D
HOMA-IR index
E
Serum TNF-α (pg/ml)
F
Serum endotoxin (EU/ml)
G
Intestinal permeability
FITC-dextran (μg/ml)
Saline
H1
DW
Clindamycin
Metronidazole
Penicillin
Vancomycin
Neomycin
ns

Supplementary figure S13

Neomycin treatment abrogates H1-mediated anti-obesogenic effects. (A) Diagram illustrating the single antibiotic treatment model used in these experiments. Saline- or H1-treated HFD-fed mice were treated with individual antibiotics in sterile drinking water (DW) for 12 weeks. Obesity traits including (B) body weight gain, (C) visceral fat pad weight, (D) HOMA-IR index, (E) serum TNF-α, (F) serum endotoxin and (G) intestinal permeability were measured after 12 weeks of treatment. Data are presented as means ± SD (n=5 mice/group) and analyzed using Student's unpaired t-test and FDR correction for multiple testing. *p<0.05; **p<0.01; ***p<0.001; ****p<0.0001; C, clindamycin; M, metronidazole; N, neomycin; ns, not significant; P, penicillin; V, vancomycin.

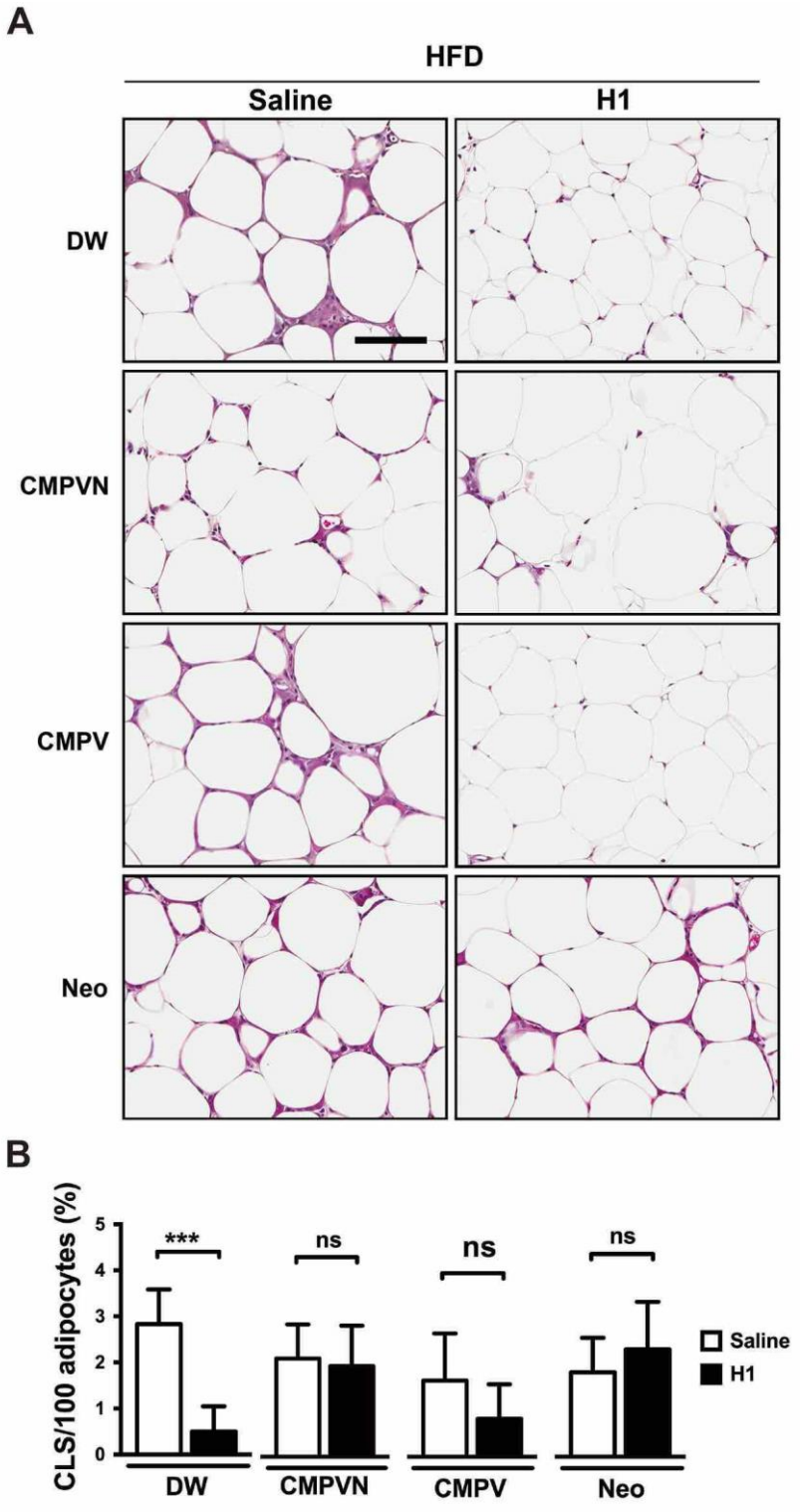

Supplementary figure S14

Neomycin treatment abrogates H1's protective effects on adipocyte hypertrophy and crown-like structures in HFD-fed mice. Experiments were performed as in figure 3. (A) Representative images of H&E-stained visceral adipose tissues. Scale bar, 100 µm. (B) Quantification of CLS (n=5 images/mouse) in visceral adipose tissues. Data represent means ± SD (n=6 mice/group) analyzed using one-way ANOVA followed by Bonferroni's post hoc test. ***p<0.001; ns, not significant.

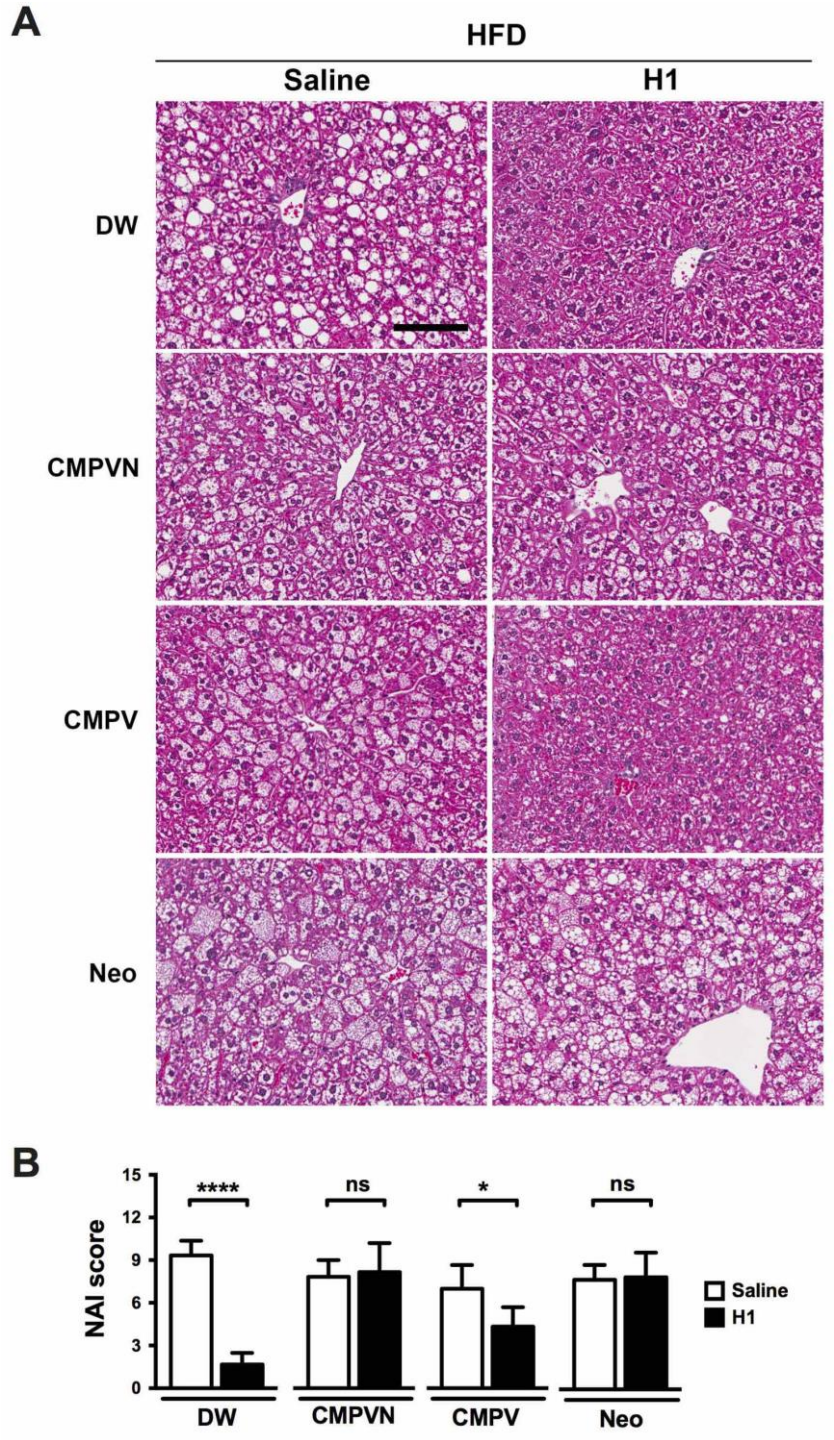

Supplementary figure S15

Neomycin treatment abrogates H1's protective effects on NAFLD and NASH in HFD-fed mice. Experiments were performed as in figure 3. (A) Representative images of H&E-stained liver tissues. Scale bar, 100 µm. (B) NAI score (n=5 images/mouse). Data represent means ± SD (n=6 mice/group) analyzed using one-way ANOVA followed by Bonferroni's post hoc test. ****p<0.0001; ns, not significant.

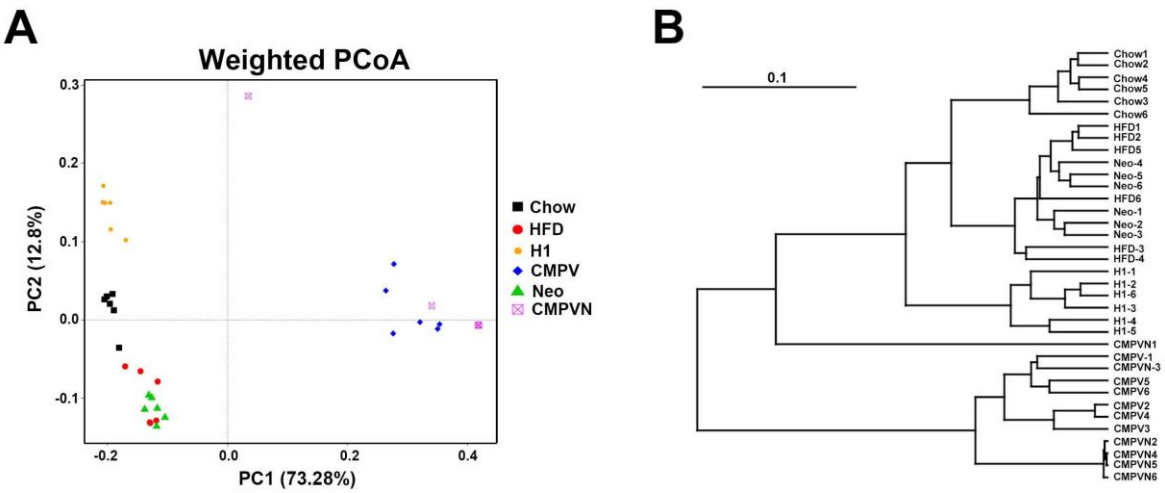

Supplementary figure S16

Clustering of gut microbiota samples based on next-generation 16S rDNA sequencing analysis. Experiments were performed as in figure 4A. (A) Plots of weighted UniFrac PCoA was prepared based on OTU abundance matrix. (B) Weighted UPGMA hierarchical clustering based on UniFrac distances (n=6 mice/group).

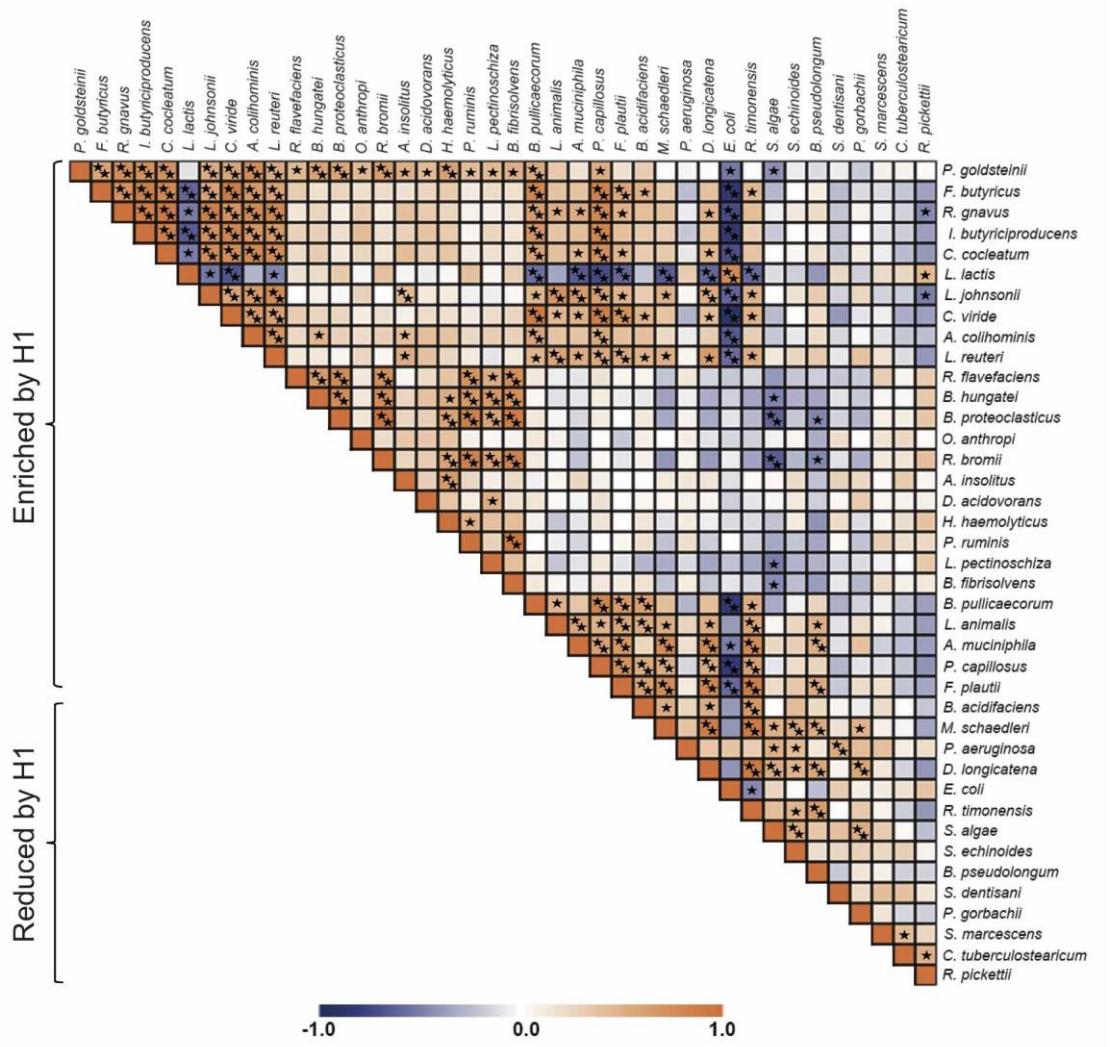

Supplementary figure S17

Interplay between H1-modulated gut bacteria. Experiments were performed as in figure 4A. Spearman correlation analysis of 40 H1-modulated gut bacterial species. Black stars indicate statistically significant difference based on Spearman correlation analysis. FDR correction for multiple testing was used. *p<0.05; ** p<0.01.

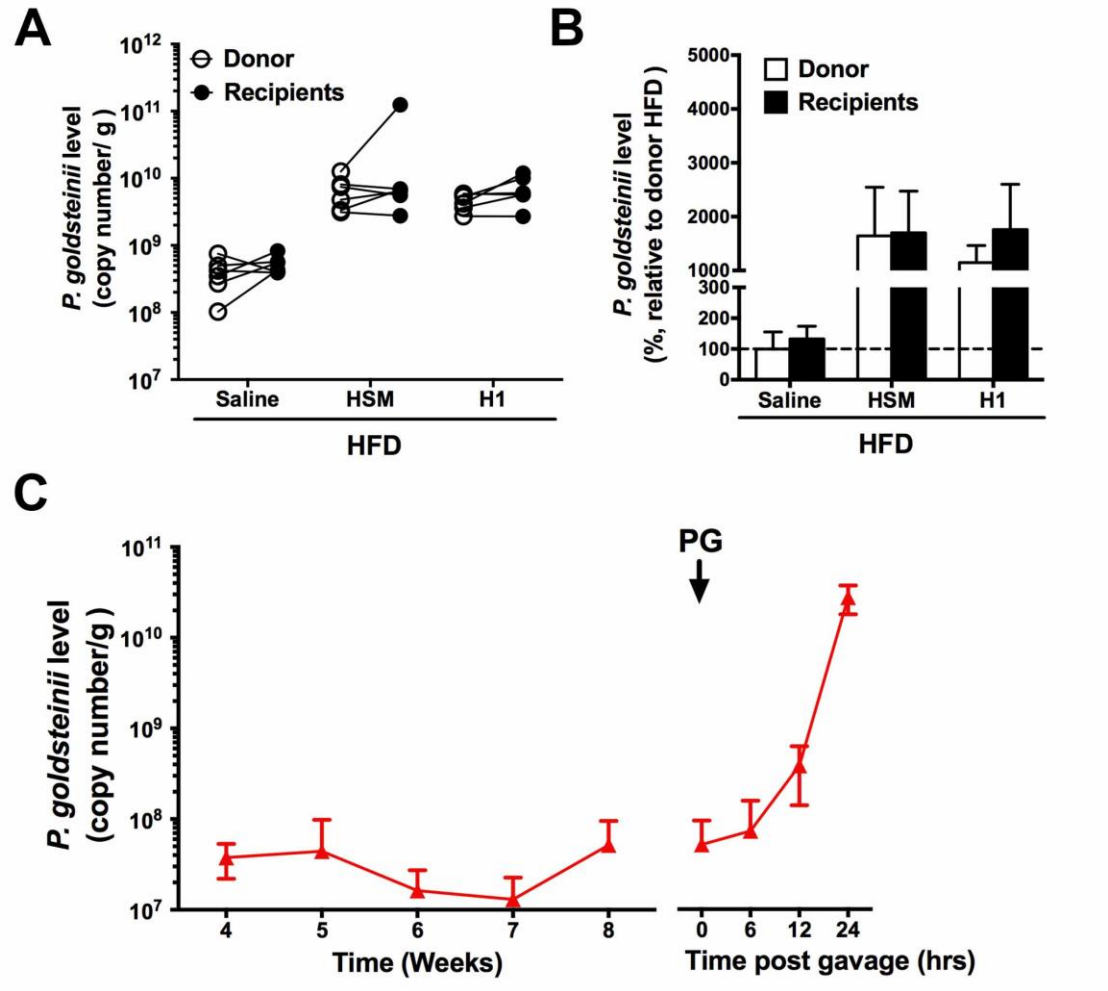

Supplementary figure S18

P. goldsteinii colonizes mice in FMT experiments. Experiments were performed as in supplementary figure S10. (A) *P. goldsteinii* levels in cecal microbiota of HFD-fed mice treated with saline, HSM or H1 and their recipients were quantified. (B) Relative levels of *P. goldsteinii* in feces of donor and recipient mice were calculated based on levels found in HFD-fed donors. (C) Colonization efficiency after a single oral gavage of *P. goldsteinii* in HFD-fed mice treated with neomycin (red line). Data are presented as means ± SD (n=5 mice/group).

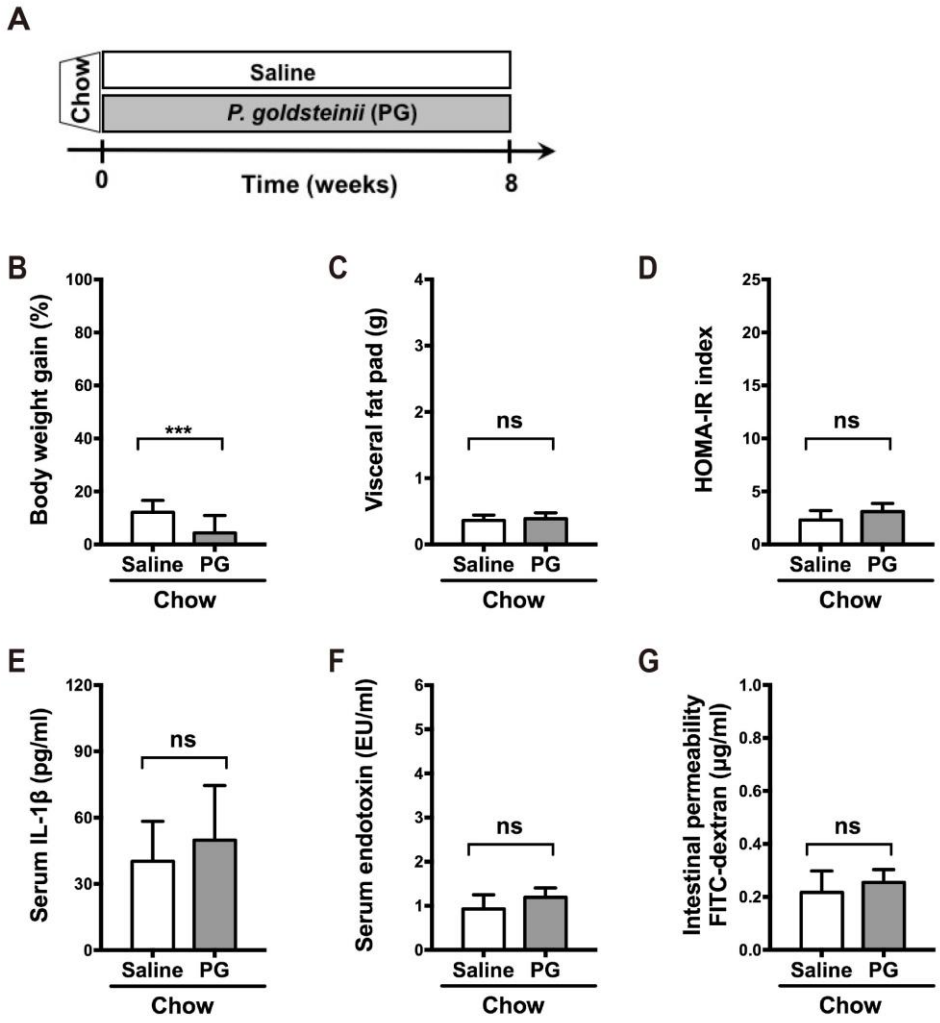

Supplementary figure S19

Effects of *P. goldsteinii* treatment in chow-fed mice. (a) Chow-fed mice were treated daily with saline or *P. goldsteinii* (PG, 4×10^7 CFUs) by oral gavage for 8 weeks. Obesity traits including (B) body weight gain, (C) visceral fat pad weight, (D) HOMA-IR index, (E) serum IL-1β, (F) serum endotoxin and (G) intestinal permeability were measured after 8 weeks of treatments. Data represent means ± SD. n=19 mice/group for panels B,C; n=6 mice/group for panels D,F,G; n=11 for panel E. Data were analyzed using one-way ANOVA followed by Bonferroni's post hoc test. ***p<0.001; ns, not significant.

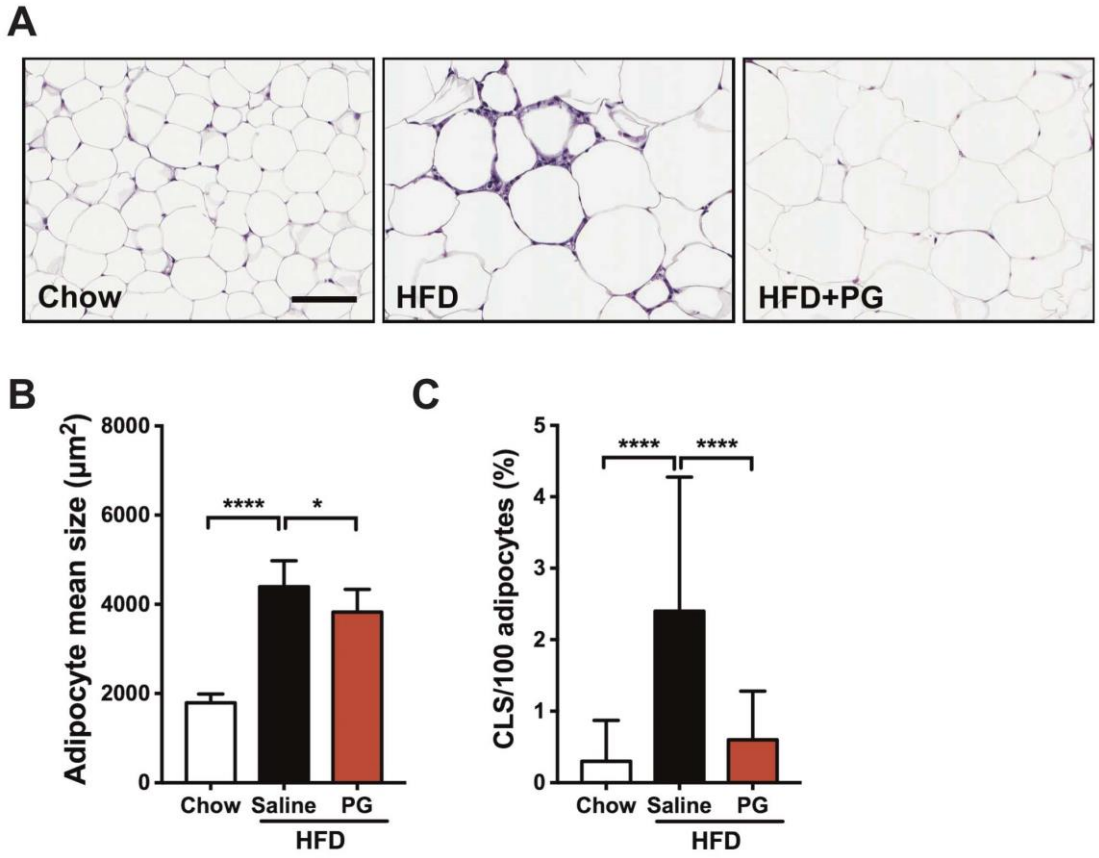

Supplementary figure S20

P. goldsteinii treatment prevents hypertrophy and crown-like structures in adipocytes of HFD-fed mice. Experiments were performed as in figure 7. (A) Representative images of H&E-stained visceral adipose tissues. Scale bar, 100 µm. (B) Adipocyte size in visceral adipose tissues was determined from five microscopy fields for each mouse using Adiposoft (Image J). Data represent medians ± IQR (n=5 mice/group). Data were analyzed using the Kruskal-Wallis test with Dunn's post hoc test. (C) Quantification of CLS (n=5 images/mouse) in visceral adipose tissues. Data represent means ± SD (n=5 mice/group). Data were analyzed using one-way ANOVA followed by Bonferroni's post hoc test. **p<0.01; ****p<0.0001.

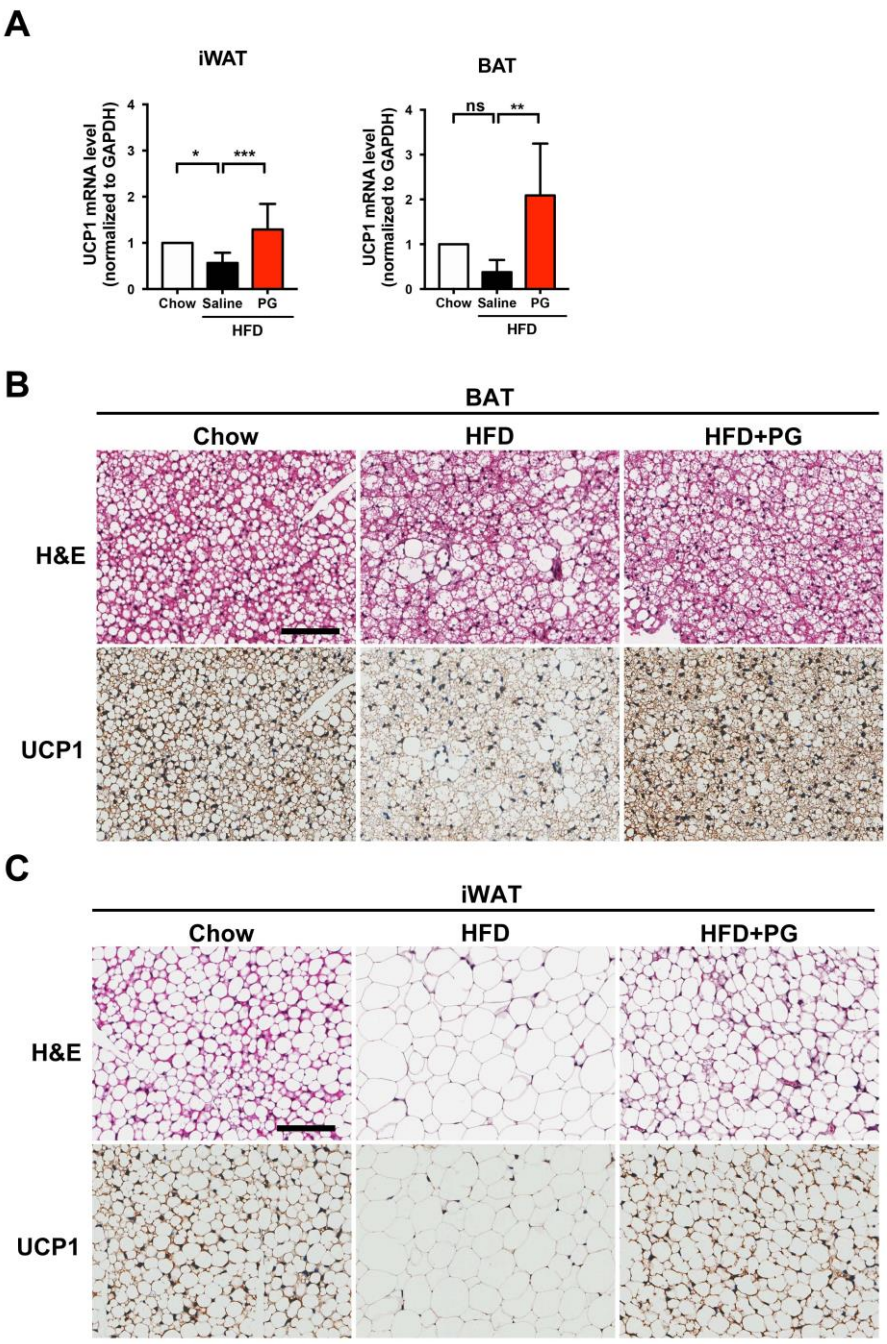

Supplementary figure S21

Live *P. goldsteinii* induces expression of thermogenic protein markers in HFD-fed mice. (A) qRT-PCR analysis of uncoupling protein 1 (UCP1) gene in BATs (left panel) and iWATs (right panel). Representative images of H&E-stained and UCP1-stained (B) BATs and (C) iWATs. Tissues slides corresponding to successive cuts were used. Scale bars, 100 µm. Data represent means ± SD (n=5 mice/group). Data were analyzed using one-way ANOVA followed by Bonferroni's post hoc test. **p<0.01; ****p<0.0001; ns, not significant.

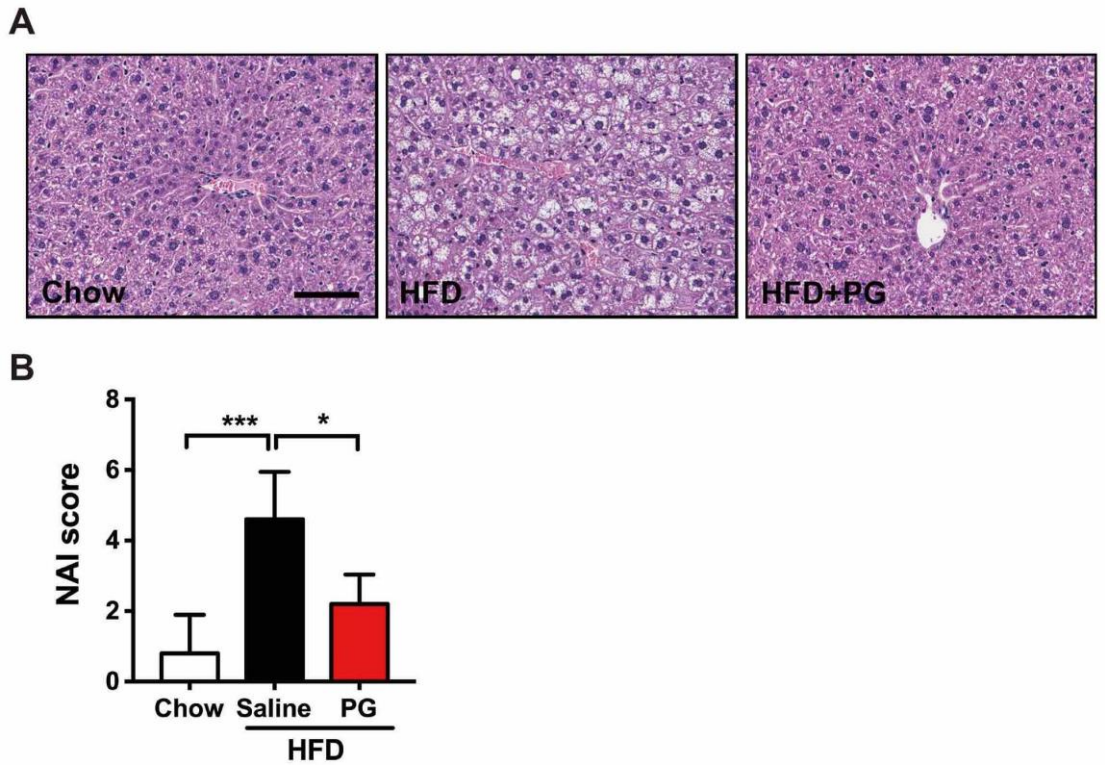

Supplementary figure S22

P. goldsteinii treatment prevents signs of NAFLD and NASH in HFD-fed mice. Experiments were performed as in figure 7. (A) Representative images of H&E-stained liver tissues. Scale bar, 100 µm. (B) NAI score. Data represent means ± SD (n=5 mice/group) and analyzed using one-way ANOVA followed by Bonferroni's post hoc test. *p<0.05; ***p<0.001.

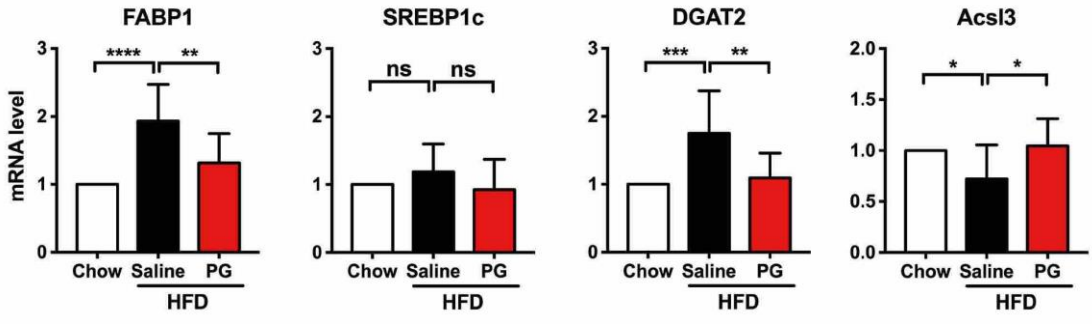

Supplementary figure S23

P. goldsteinii treatment normalizes gene expression involved in lipid metabolism in HFD-fed mice. Experiments were performed as in figure 6. Expression of lipid metabolism genes in the liver, including FABP1, SREBP1c, DGAT2 and Acsl3, was evaluated using qRT-PCR. Data represent means ± SD (n=8 to 11 mice/group). Data were analyzed using one-way ANOVA followed by Bonferroni's post hoc test. *p<0.05; **p<0.01; ***p<0.001; ****p<0.0001; ns, not significant.

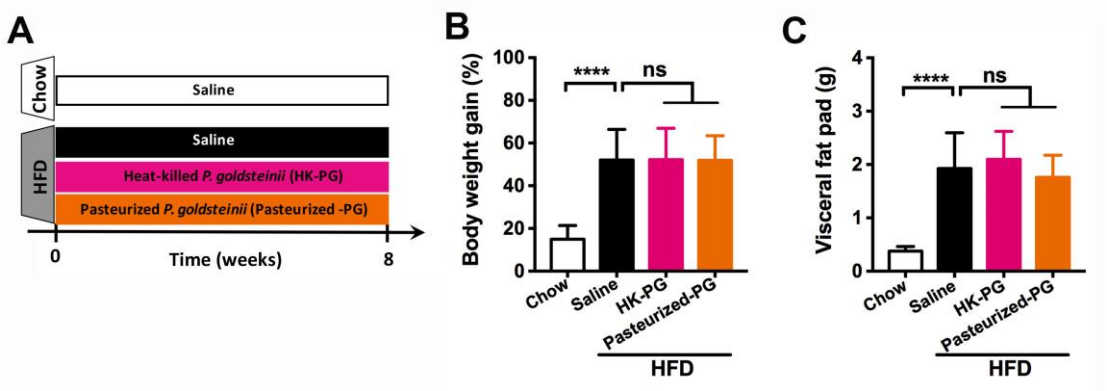

Supplementary figure S24

Heat-killed and pasteurized *P. goldsteinii* fail to prevent obesity in HFD-fed mice. (A) Chow-fed mice and HFD-fed mice were treated daily with saline, heat-killed (HK-PG) or pasteurized *P. goldsteinii* (4×10^7 CFUs each) by oral gavage for 8 weeks. (B) Body weight gain and (C) visceral fat pad weight were monitored after 8 weeks of treatment. Data represent means ± SD (n=10–15 mice/group). Data were analyzed using one-way ANOVA followed by Bonferroni's post hoc test. ****p<0.0001; ns, not significant.

Supplementary table S1

Molecular weight analysis of fractions isolated from HSM water extract

Fraction	Main Compound	Molecular Weight (kDa)	Percentage (%)
H1	Polysaccharides	>300	20.1
H2	Polysaccharides	10–300	30.6
H3	Polysaccharides	<10	7.7
H4	Mono-, di-, oligosaccharides	Undetermined	39.7

Polysaccharides were analyzed from 100 ml of HSM water extract. Shown in the last column are the percentages that each fraction represents based on the total HSM water extract.

Supplementary table S2

Biochemistry analysis of serum of mice treated with *P. goldsteinii* for 8 weeks

Parameters	Chow[a]		HFD	
	Saline	PG	Saline	PG
AST (U/l)	73.89±13.38	76.59±11.19	107.92±31.82*	80.95±17.32[#]
ALT (U/l)	28.66±7.21	26.34±4.98	49.5±30.52*	34.54±13.89
T-BIL (µg/dl)	29.65±6.14	25.12±4.02	43.22±14.38	40.43±13.1
ALB (g/dl)	3.04±0.14	3.09±0.17	2.95±0.19	2.96±0.05
BUN (mg/dl)	32.98±11.79	28.26±2.93	18.4±3.63*	21.88±2.96
CREA (mg/dl)	0.26±0.14	0.21±0.05	0.19±0.05	0.21±0.05
UA (mg/dl)	3.54±2.04	3.28±2.4	2.1±1.83	2.16±1.31

[a]Data represent means ± SD of duplicate experiments (n=6 to 10 mice/group) in mice fed with chow or HFD and orally treated with saline or *P. goldsteinii* (PG; 4×10^7 CFUs).

*Values showing a statistically significant difference ($p<0.05$) compared with the chow-saline group.

[#]Indicates a statistically significant difference ($p<0.05$) compared with the HFD-saline group.

Data were analyzed using one-way ANOVA followed by Bonferroni's post hoc test.

AST, aspartate aminotransferase; ALT, alanine aminotransferase; T-BIL, total bilirubin; ALB, albumin; BUN, blood urea nitrogen; CREA, creatinine; UA, uric acid.

Supplementary table S3

Monosaccharide composition of polysaccharide fraction H1

	Man	Glc	Gal	GlcN	Ara	GalN	Rha	Fuc
Concentration (%)	50.4	12.5	23.8	4.6	1.7	0.4	3.4	3.2

Man, mannose; Glc, glucose; Gal, galactose; GlcN, N-glucosamine; Ara, arabinose; GalN, N-galactosamine; Rha, rhamnose; Fuc, fucose.

Supplementary table S4

PCR primers used in this study

Target	Direction	Primer sequence (5'–3')
Mouse genes		
IL-1β[23]	Forward	TTGAAGAAGAGCCCATCCTC
	Reverse	CAGCTCATATGGGTCCGAC
TNF-α[23]	Forward	TAGCCAGGAGGGAGAACAGA
	Reverse	TTTTCTGGAGGGAGATGTGG
ZO-1[23]	Forward	ACCCGAAACTGATGCTGTGGATAG
	Reverse	AAATGGCCGGGCAGAACTTGTGTA
CD36[24]	Forward	ATGGGCTGTGATCGGAACTG
	Reverse	GTCTTCCCAATAAGCATGTCTCC
Fasn[25]	Forward	GCTGCGGAAACTTCAGGAAAT
	Reverse	AGAGACGTGTCACTCCTGGACTT
HSL[26]	Forward	GCTGGGCTGTCAAGCACTGT
	Reverse	GTAACTGGGTAGGCTGCCAT
LPL[27]	Forward	GGACGGTAACGGGAATGTATG
	Reverse	ACGTTGTCTAGGGGGTACTTAAA
FABP1[28]	Forward	TGGACCCAAAGTGGTCCGCA
	Reverse	AGTTCAGTCACGGACTTTAT
SREBP1c[29]	Forward	GATGTGCGAACTGGACACAG
	Reverse	CATAGGGGGCGTCAAACAG
DGAT2[30]	Forward	ATCTTCTCTGTCACCTGGCT
	Reverse	ACCTTTCTTGGGCGTGTTCC
Acsl3[31]	Forward	GGGACTACAATACCGGCAGA
	Reverse	ATAGCCACCTTCCTCCCAGT
UCP1[32]	Forward	AGGCTTCCAGTACCATTAGGT
	Reverse	CTGAGTGAGGCAAAGCTGATTT
GAPDH[23]	Forward	GCATCCACTGGTGCTGCC
	Reverse	TCATCATACTTGGCAGGTTTC

Human genes		
ZO-1[33]	Forward	GCAGCTAGCCAGTGTACAGTATAC
	Reverse	GCCTCAGAAATCCAGCTTCTCGAA
18S[34]	Forward	GTAACCCGTTGAACCCCATT
	Reverse	CCATCCAATCGGTAGTAGCG
Other genes		
16S rDNA 27F-1492R[35]	Forward	AGAGTTTGATCCTGGCTCAG
	Reverse	GGTTACCTTGTTACGACTT
P. goldsteinii	Forward	GAATAAAGTGAGGAACGTGTT
	Reverse	AACTTTCACCGCTGACTTAATTA
16S rDNA 520R[35] (for cloning sequencing)	Reverse	ACCGCGGCTGCTGGC

Supplementary datasets

Supplementary dataset S1

(Microsoft Excel file). Non-alcoholic steatohepatitis activity index (NAI) assessment.

Supplementary dataset S2

(Microsoft Excel file). Reads generated from next-generation sequencing of each mouse in in vivo antibiotic mouse experiments. Related to figure 4.

Supplementary dataset S3

(Microsoft Excel file). Relative abundance of bacterial species showing differences between the H1-treated group and antibiotics groups after HFD feeding for 12 weeks. Related to figure 4A,B.

Supplementary dataset S4

(Microsoft Excel file). Spearman correlation analysis between the bacterial species identified and obesity traits. Related to figure 4D.

Supplementary dataset S5

(Microsoft Excel file). Relative abundance of bacterial species showing differences between the H1-treated donor group and antibiotics donor groups after HFD feeding for 12 weeks. Related to figure 6A,B.

Supplementary dataset S6

(Microsoft Excel file). Relative abundance of bacterial species showing differences between the H1-treated recipient group and antibiotics recipient groups after HFD feeding for 12 weeks. Related to figure 6C,D.


bsg
BRITISH SOCIETY OF
GASTROENTEROLOGY
BMJ Journals